~~Analysis~~ Meteorological history of ~~multi-seasonal meteorological storylines leading to reduced~~ low forest greenness events in Europe in ~~2000-2020~~2002–2022

Mauro Hermann[1], Matthias Röthlisberger[1], Arthur Gessler[2,3], Andreas Rigling[2,3], Cornelius Senf[4], Thomas Wohlgemuth[2], and Heini Wernli[1]

[1]Institute for Atmospheric and Climate Science (IAC), ETH Zürich, Zurich, Switzerland
[2]Swiss Federal Institute for Forest, Snow and Landscape Research (WSL), Birmensdorf, Switzerland
[3]Institute of Terrestrial Ecosystems (ITES), ETH Zürich, Zurich, Switzerland
[4]Ecosystem Dynamics and Forest Management Group, Technical University of Munich, Freising, Germany

Correspondence: Mauro Hermann (mauro.hermann@env.ethz.ch)

Abstract.

~~Recent forest decline in Europe~~ Forest dieback in Europe has recently intensified and become more extensive. This dieback is strongly influenced by meteorological ~~conditions imposed by seasonal~~ variations of temperature, $T2m$, and precipitation, P, and can be monitored with forest greenness. This study quantitatively investigates ~~anomalous characteristics of~~ the three-year meteorological ~~storyline~~ history preceding events of reduced forest greenness in Europe's temperate and Mediterranean biome ~~in the phase space of seasonal-mean anomalies of ($T2m, P$)~~with a systematic approach. A specific focus ~~is on the amplitude, persistence, and co-variability of these anomalies~~ lies on the timing of unusually persistent and of unusually strong anomalies of $T2m$ and P, as well as their relation to synoptic weather systems. A pragmatic approach based on remote sensing observations of normalized difference vegetation index $NDVI$ serves to identify low forest $NDVI$ events at the 50 km scale in Europe in June to August ~~2000~~2002–~~-2020. An independent forest disturbance data set is used to qualitatively validate the identified more than 1'500~~ -2022. We quantify the impact of the hottest summer on record in Europe in 2022, which, according to our criteria, negatively affected 37% of temperate and Mediterranean forest regions, and thereby reduced forest greenness more extensively than any other summer in 2002–2022.

The low $NDVI$ events ~~. These events occur in summers with~~ occurred in particularly dry and hot ~~conditions~~ summers but their meteorological ~~storylines feature significant anomalies during multiple seasons preceding the events~~histories featured also significant anomalies further in the past, with clear differences between the ~~two biomes. In the Mediterranean biome, the anomalously dry conditions persist over more than 1.5 y prior to the events, whereas $T2m$ is anomalously warm only during the last 0.4 y. In contrast, in~~ temperate and Mediterranean biome. A key feature is the anomalous accumulation of dry periods (i.e., periods with a P deficit) over the preceding 26 and 34 months in the temperate and Mediterranean biome, respectively. In the temperate biome only, $T2m$ ~~is anomalously large during most of the 2.5 y prior to the events and , most interestingly, the autumn/winter preceding the events is characterized by anomalously wet and warm conditions . These anomalies potentially induce a negative legacy on the following summerdrought. The seasonal-mean anomalies of P are~~

~~strongly determined by synoptic-scale weather systems, such that long dry periods are characterized by a deficit of cyclones and an excess of anticyclones. A final analysis investigates the peculiarities of low~~ was anomalously persistent during almost the same 26-month period and featured distinctive peaks late in the past three growing seasons. While anomalously strong hot-dry conditions were characteristic for temperate low $NDVI$ ~~events that occur in two consecutive summers and the potential role of drought legacy effects. In the~~ events already in the previous summer, we find hardly any other systematic meteorological precursor in the Mediterranean prior to the event year. The identified dry periods went along with reduced cyclone activity in the Mediterranean, and positive anticyclone frequency in the temperate biome, ~~the second event summer of an event sequence has less hot and less dry anomalies than the first one and than during a single event .~~ respectively. The occurrence of these two weather systems is locally more nuanced, showing, e.g., consistently increased and decreased cyclone frequency over western and northern Europe, respectively, in all event summers. Finally, the systematic meteorological histories are useful to test whether locally observed meteorological impacts, e.g., structural overshoot, systematically influenced the investigated events. In summary, ~~detailed~~ systematic investigations of the multi-annual meteorological ~~storyline of low forest $NDVI$ events~~ history provided clear evidence ~~that anomalies of~~ of how surface weather and synoptic-scale weather systems over ~~time periods of up to 2.5 y~~ up to three years can negatively impact European forest ~~activity, with important differences between the temperate and Mediterranean biomes~~greenness. The observation of the record-extensive low $NDVI$ event in summer 2022 underlines that understanding the forest-meteorology interaction is of particular relevance for forest dieback in a changing climate.

1 Introduction

European forest ecosystems have typically been in balance with their ~~bio-physical~~ climatic environment and are, thus, largely adapted and acclimated to ~~the local mean climate and its variability~~ meteorological variability on a larger scale. This balance is increasingly disturbed by anthropogenic climate change (Seidl et al., 2017; McDowell et al., 2020). As a consequence, the exposure and vulnerability of European forests to climatic disturbances has increased in the recent two decades and forests were affected on up to the continental scale (Seidl et al., 2014; Bastos et al., 2020b). On ~~the continental~~ that scale, drought has been a key driver of excess forest mortality in Europe (Senf et al., 2020). In addition to meteorological drought, i.e., reduced precipitation, high temperatures enhance the atmospheric water demand and, thus, water loss from the vegetated surface by evapotranspiration (Yuan et al., 2019; Grossiord et al., 2020). Heatwaves (Meehl and Tebaldi, 2004; IPCC, 2021), meteorological droughts (Trenberth et al., 2014; IPCC, 2021), and compound hot droughts (Allen et al., 2015) are expected to intensify future forest ~~decline~~ dieback (Brodribb et al., 2020). Such meteorological conditions, for example during 2003 and 2018, led to stem dehydration (Salomón et al., 2022), reduced forest growth (Ciais et al., 2005; Trotsiuk et al., 2020), ~~complete~~ hydraulic failure (Schuldt et al., 2020), and ultimately increased tree mortality in Europe (Allen et al., 2010; Hansen et al., 2013). ~~At the same time, recent hot-dry conditions fostered bark beetle outbreaks (Rouault et al., 2006; Jakoby et al., 2019) and forest fires (Seidl et al., 2017).~~ Although some forest ecosystems are adapted to low ~~summer water availability~~ water availability in summer, e.g., in the summer-dry Mediterranean~~or~~ , or throughout the year, e.g., in dry inner-Alpine regions, extended and more frequent hot droughts will strongly affect their dynamics including growth and survival (Rigling et al., 2013; Tague et al., 2019; Ogaya et al., 2020). In this context, forest greenness as measured by satellites is an effective measure related to forest ~~performance~~ vitality to monitor the recent forest ~~decline~~ dieback in Europe (Orth et al., 2016; Buras et al., 2020, 2021).

While forests can endure short-term weather extremes (e.g., an individual multi-day heatwave), they are more susceptible to longer-term extreme conditions. Particularly harmful long-term extremes include persisting or sequentially occurring droughts~~that disturb forests beyond the summed individual impacts, as the initial drought exerts a negative legacy effect on the following one by reducing forest~~, whereby additional negative legacy effects are mediated through reduced tree resilience (Anderegg et al., 2015, 2020; Bose et al., 2020). However, drought legacy effects have also been suggested to provide acclimation to following droughts (Gessler et al., 2020). ~~Moreover, compound hot and dry periods cause an impact exceeding that of the summed uni-variate extremes (Zscheischler and Seneviratne, 2017).~~ Furthermore, a stormy winter followed by a hot-dry growing season allows bark beetles to spread out and attack damaged and dying trees (Temperli et al., 2013; Biedermann et al., 2019; Jakoby et al., 2019). Additionally, persisting heat, and/or precipitation deficits can – given fuel availability – trigger forest fires year-round, occurring most intensely in the Mediterranean (Turco et al., 2017). In strongly fuel-limited regions, however, forest fires can in the long run negatively feed back on fire activity (Pausas and Ribeiro, 2013). Lastly, beneficial conditions in the ~~early growing season~~ past can exert a negative legacy on forest ~~activity in dry summers, as early growth fosters canopy buildup and~~ vitality in following dry periods through soil moisture depletion ~~(Bastos et al., 2020a).~~and structural overshoot, i.e., an excessive canopy buildup relative to average climatic conditions (Bastos et al., 2020a; Zhang et al., 2021). These examples highlight that in addition to the (co-)occurrence, magnitude, and duration of heat and drought, ~~their position in a~~ the position of such meteorological precursors in the longer-term ~~meteorological storyline modulates their interplay with other disturbances and, thus, also their~~ history likely modulates their impact on forest ~~performance~~greenness.

In the context of ~~such interactions~~ interaction and legacy effects the ~~time-scale over which the meteorological storyline is~~ point in time when such meteorological precursors are relevant to forest ~~performance~~ greenness is intensively discussed ~~. The meteorological~~ in the literature. Meteorological impact has often been investigated by considering the mean over the current growing season (e.g., Hlásny et al., 2017; Seftigen et al., 2018; Seidl et al., 2020). ~~A recent comprehensive analysis of drought-induced canopy mortality~~ Senf et al. (2020) revealed that hot-dry conditions are particularly harmful for canopy mortality in March to July~~(Senf et al., 2020). Neumann et al. (2017) stressed~~. Neumann et al. (2017) identified warm summer temperatures and high variability in seasonal precipitation as meteorological drivers of tree mortality. In a drought-prone region, forest drought stress was about equally determined by temperature in summer and the previous autumn, and precipitation during the cold season (Williams et al., 2013). More generally, drought-induced partial or complete tree mortality shows a threshold behaviour (Brodribb et al., 2020; Senf et al., 2020); however, water stress is not equally harmful at all times. Especially outside or at the ~~margins~~ bounds of the growing season there are complicating factors such as growth compensation, soil moisture coupling, and snow melt (e.g., Harpold et al., 2015; Bastos et al., 2020a).~~Despite increasing understanding, a systematic analysis of the meteorological storyline of reductions in forest performance in Europe is still missing.~~

The meteorological processes that are relevant for low forest ~~performance~~ greenness cover a wide range of timescales. ~~Although longer-term~~ Longer-term meteorological extremes are of particular interest, ~~they can also be~~ however, they are typically composed of multiple shorter-term anomalies, which are not necessarily extreme at ~~that~~ their respective timescale (Röthlisberger et al., 2020). On the timescale of about 3–10 days, atmospheric blocking can induce surface heatwaves and suppress precipitation by large-scale subsidence and high solar insulation (Pfahl and Wernli, 2012a; Zschenderlein et al., 2019). ~~At the same time , the involved~~ On somewhat longer time scales, recurrent and quasi-stationary ~~upper-tropospheric ridge leads to reduced precipitation~~Rossby wave patterns may also lead to co-occurring hot and dry conditions (Wolf et al., 2018; Röthlisberger and Ma In central Europe, summer heatwaves can also arise from weak synoptic forcing, which, in combination with a Scandinavian blocking, allowed for widespread hot-dry conditions in 2018 (Spensberger et al., 2020). During heatwaves with no or reduced precipitation, the soil moisture-atmosphere coupling exacerbates the near-surface warming over drying soils (Fischer et al., 2007; Seneviratne et al., 2010). Accordingly, and especially in the Mediterranean, an extremely hot summer is more likely in years of a winter/spring precipitation deficit ~~(Russo et al. , 2019).~~ (Russo et al., 2019). As Europe hardly experiences drought over a longer (multi-annual) time scale (Schubert et al., 2016), seasonal meteorology, which is strongly linked to weather system dynamics, is of particular interest for forest ~~performance~~greenness, and, therefore, in the focus of the present study.

Despite great progress in understanding the eco-hydraulic mechanisms linking drought to events of reduced forest ~~performance and, thus,~~ greenness (Brodribb et al., 2020), a systematic analysis of ~~meteorological storylines accompanying~~ the meteorological history of such events is still lacking. The purpose of this study is to systematically document and characterize ~~these meteorological storylines~~ significant aspects of these meteorological histories in Europe's temperate and Mediterranean forests. Specifically, this study seeks to identify meteorological precursors over the three years prior to reduced forest greenness in Europe. Hereby "precursors" are features in the meteorological histories that occur at a statistically significantly higher rate preceding reduced forest greenness events than in climatology, and that are shared among many events. We focus on the evolution of 90-day average 2-m temperature ($T2m_{90d}$) and precipitation (P_{90d}) as key ~~characteristics of the three-year meteorological storylines~~ variables and quantitatively address the following research questions~~in Sect. 3.3~~: (1) ~~What is the average meteorological storyline preceding~~ When and how deviated $T2m_{90d}$ and P_{90d} significantly from climatology during the meteorological history of low forest greenness events in Europe~~'s temperate and Mediterranean forests~~? (2) ~~How anomalous is the magnitude and persistence of $T2m_{90d}$ and P_{90d} anomalies at different time lags prior to the events? (3) Which changes~~ Which anomalies in weather system ~~frequency go~~ frequencies went along with the meteorological ~~storyline~~ precursors identified in (1)? ~~(4) How does the meteorological storyline differ for sequences of~~ To identify low forest greenness events~~as compared to single events? To do so, we use~~ , generally characteristic for low productivity crown defoliating and tree mortality (Buras et al., 2021), we use persistently low values of the normalized difference vegetation index ($NDVI$) in summer ~~2000–2020 as a measure of reduced forest greenness~~ 2002–2022 (Sects. 2.2 & 2.3). ~~We also aim to answer whether the identified~~ Based on a sub-sampling of the resulting low $NDVI$ events ~~feature more forest disturbances than non-events by evaluating them with a more comprehensive European forest disturbance data set by Senf and Seidl (2021a, Sect. ??).~~ in combination with a bootstrapping test, we then identify meteorological precursors along their meteorological history, and further investigate the spatial variation of weather system frequencies in Sect. 3. Finally, we critically discuss our results and the limitations of our analyses in Sect. 4.

~~The term "meteorological storyline" is central to this study. It encompasses the evolution of P_{90d} and $T2m_{90d}$ over the three years prior to low $NDVI$ events, and, thereby, emphasizes the two fundamental meteorological variables at the seasonal time scale. Throughout the story we focus on different periods within, and use various measures of the meteorological storyline, respectively, e.g., anomalies of P_{90d} and $T2m_{90d}$ or their bi-variate evolution, to capture all its facets.~~

2 Data and methods

We differentiate broadly between the temperate and Mediterranean biome according to Schultz (2005) in the domain extending from 10° W to 45° E and 35° N to ~~60~~65° N, excluding all boreal forests (Fig. 1a).

~~(a) forest grid cells in the study domain, separated into temperate and Mediterranean forests by the black dashed line. The boreal biome is cropped by the second dashed line in the Northeast of the domain. Hatching indicates where events cannot be evaluated with the disturbance data set (see Sect. ??). (b) the identification of low $NDVI$ events in an example forest grid cell (details provided in the text).~~

2.1 Forest cover data

~~Forest~~ Land surface cover observations are available from the ~~global tree canopy cover data version 1.7 derived from Landsat at one arc-second (~30 m)~~ Corine Land Cover (CLC) data set from the Copernicus Land Monitoring Service at 100 m horizontal resolution from the year ~~2000 (Hansen et al., 2013)~~2018 (Büttner et al., 2004). For comparison with the other data sets introduced below, we first interpolate the surface cover to 250 m resolution by nearest-neighbor interpolation. Following that, we mask all pixels except forest land cover classes (coniferous, broad-leaved, and mixed forest) to retain only forest pixels. We then coarse grain fractional forest area to $0.5° \times 0.5°$ grid cells, which is the spatial resolution of the meteorological data set used here (ERA5, see below), ~~FA, to 0.05° (~5 km)and to 0.5° (~50 km),~~ hereafter denoted as ~~$FA^{0.05}$ and~~ $FA^{0.5}$~~, respectively~~. For our analysis we only consider ~~sufficiently forest-covered 0.05°×0.05° pixels, i.e., pixels with $FA^{0.05} \geq 50\%$, termed forest pixels. We additionally request that they lie within 0.5°×0.5°~~ grid cells with a significant fraction of forest cover, defined here as $FA^{0.5} \geq FA^{min} = 10\%$, and hereafter refer to these grid cells as "forest ~~coverage $FA^{0.5} \geq 20\%$, termed forest~~ grid cells". According to this definition, there are 1'~~387 and 343~~ 260 and 544 forest grid cells in the temperate and Mediterranean biome, respectively ~~, as shown in~~ (Fig. 1a).

2.2 Normalized difference vegetation index

We use the ~~monthly~~ 16-daily normalized difference vegetation index ($NDVI$) at ~~0.05°~~ ~250 m horizontal resolution from ~~February 2000 to August 2020~~ March 2002 to August 2022 from NASA MODIS Terra ~~provided on the Giovanni data system (Acker and Leptoukh, 2007)~~(Didan, 2015). It is based on the red (RED) and near-infrared (NIR) spectral irradiance:

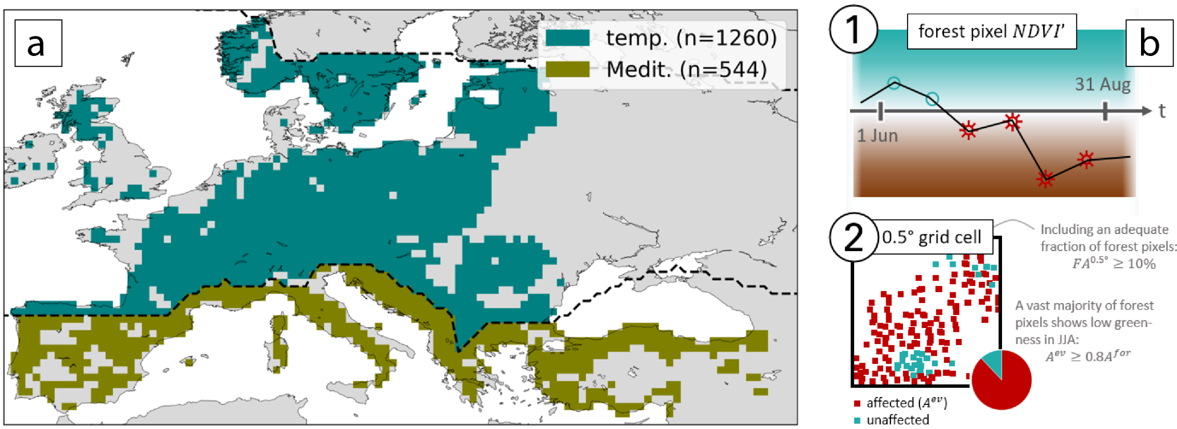

Figure 1. (a) forest grid cells ($FA^{0.5} \geq 10\%$) in the study domain, separated into temperate and Mediterranean forests by the black dashed line. The boreal biome is cropped by the second dashed line in the Northeast of the domain. (b) an example of the identification of low $NDVI$ grid cells, where (1) forest pixels are flagged if at least 4/6 time steps show negative $NDVI'$, and (2) $0.5° \times 0.5°$ forest grid cells are flagged if more than 80% of the forest pixels within are flagged (details provided in the text).

$$NDVI = \frac{NIR - RED}{NIR + RED} \tag{1}$$

The greener a vegetated surface is, the closer its $NDVI$ is to +1 (Tucker, 1979). ~~Note that at forest pixels, the $NDVI$ additionally depends on the remaining vegetation cover, i.e., on within-pixel heterogeneity in surface reflectance properties.~~ The $NDVI$ serves as a measure of vegetation ~~performance~~ greenness and has previously been used to assess drought impact on ecosystems (Anyamba and Tucker, 2012; Orth et al., 2016; Buras et al., 2020). ~~We linearly interpolate missing values from the previous and subsequent month, and~~ The Application for Extracting and Exploring Analysis Ready Samples (AppEEARS) additionally provides MODIS pixel quality. We mask $NDVI$ values that are of poor quality due to snow and clouds, and only retain $NDVI$ values with good and marginal quality according to MODIS pixel quality. The resulting $NDVI$ time series contain missing values, which we linearly interpolate from neighbouring time steps as in Buras et al. (2021). Finally, we perform a linear detrending of the entire time series as in Buras et al. (2020) due to a detected greening trend (Bastos et al., 2017).~~Gap interpolation is mainly necessary over water and hardly affects our analysis.~~

After this post-processing, ~~we only consider normalized~~ at every pixel j at time step t in year n we consider $NDVI$ anomalies (~~$NDVI'$) at forest pixels and~~ $NDVI'_{j,t,n}$) from the median in June–August (JJA). ~~At every forest pixel j in month m and year n, $NDVI'_{j,mn}$ results from dividing the absolute anomaly~~ To later compare anomalies at different pixels, we standardize the anomalies by the local ~~standard deviation $\sigma_j(NDVI)$, which is calculated from all 63 monthly $NDVI$~~

~~anomalies in JJA 2000–2020. The respective climatology $\overline{NDVI_{j,m}}$ is calculated as the mean in 2000–2020.~~ inter-quartile range $IQR_j(NDVI)$:

$$NDVI'_{\cancel{j,mn}\,j,t,n} = \cancel{\frac{NDVI_{j,mn}-\overline{NDVI_{j,m}}}{\sigma_j(NDVI)}}\ \frac{NDVI_{j,t,n}-\overline{NDVI_j}}{IQR_j(NDVI)} \tag{2}$$

~~Note that $\sigma_j(NDVI)$ is merely used as a measure of inter-annual~~ The climatological median $\overline{NDVI_j}$ and $IQR_j(NDVI)$ are both calculated from all 126 $NDVI$ ~~variability in JJA, and not for quantifying the likelihood or the return period of a given value. The normalization is used here because the short data record precludes more sophisticated statistical modelling, and , at least to some extent, enables comparisons of $NDVI$ values across Europe and over the study period. Also, according to a Shapiro-Wilk test, the assumption of normally distributed $NDVI$~~ anomalies in JJA ~~2000–2020, which is implicit to normalization, cannot be rejected at 72% of all forest pixels (p-value > 0.05)~~2002–2022.

2.3 Identification of low $NDVI$ ~~events~~grid cells

The aim of the ~~scheme~~ approach presented here is to identify persistently low $NDVI$ ~~events at $0.5° \times 0.5°$ forest grid cells, as this is the resolution~~ in JJA at the relatively large 0.5° scale of the meteorological ~~data used in this study (see below).~~reanalysis data, i.e., wide-spread low $NDVI$. In essence, ~~it~~ the approach (1) considers all forest pixels j within a forest grid cell J and flags them if ~~their~~ at least four out of the six $NDVI'$ ~~is below a specified threshold~~values in JJA are negative, and (2) identifies an event ~~in~~ at forest grid cell J ~~if the majority~~ (i.e., a $0.5° \times 0.5°$ grid cell with at least 10% forest cover) if at least 80% of forest pixels inside J ~~is~~ are flagged (Fig. 1b). Our identification scheme thus features three tuning parameters: (1) the FA^{min}, (2) the minimum number of negative $NDVI'$ per JJA at the pixel level ($n_{t,ev}^{min}$), and (3) the fraction of affected forest pixels per forest grid cell. An extensive sensitivity analysis to reasonable variations in these parameters is presented in Appendix A. Hereafter we detail the technical implementation of the approach.

In the first step (1 in Fig. 1b), we ~~calculate the annual minimum of the three $NDVI'_{j,mn}$ values in JJA of~~ count the number of negative $NDVI'_{j,t,n}$ values for the six 16-daily values during JJA in year n~~, termed $NDVI'^{min}_{j,n}$~~. At every forest pixel j, an event flag $ev_{j,n}$ is determined according to the following criterion:

$$ev_{j,n} = \begin{cases} 1 & \text{if } NDVI'_{j,t,n} < 0 \text{ for } n_{t,ev} \geq n_{t,ev}^{min} = 4;\ t \in \{1,2,...,6\}, \\ 0 & \text{otherwise.} \end{cases} \tag{3}$$

In the second step (2 in Fig. 1b), ~~we check whether more than half of the forest pixels in J are flagged as $ev_{j,n} = 1$. Therefore, the~~ the total area of forest pixels with $ev_{j,n} = 1$ in J ($A^{ev}_{J,n}$) has to be at least ~~50~~80% of the total forest pixel area in J (A^{for}_J) - for which we use the term minimum affected ratio $AR^{min} = 80\%$ hereafter:

$$EV_{J,n} = \begin{cases} 1 & \text{if } A^{ev}_{J,n} \geq 0.8 A^{for}_J, \\ 0 & \text{otherwise.} \end{cases} \tag{4}$$

~~For~~ Lastly, for the identified low $NDVI$ ~~events ($EV_{J,n}=1$)~~grid cells, we calculate a measure of event intensity ~~. It is equal to the spatial average of summer minimum $NDVI'^{min}_{j,n}$ at~~ as the average of JJA minimum $NDVI'_{j,t,n}$ over all flagged forest pixels ($ev_{j,n}=1$), and, hereafter, termed $NDVI'^{min}_{J,n}$. Subscripts are omitted whenever possible without loss of clarity.

The resulting low $NDVI$ grid cells ($EV_{J,n}=1$) are tested for their sensitivity to the three threshold parameters AR^{min}, FA^{min}, and $n^{min}_{t,ev}$ in Appendix A. Our choice of $AR^{min}=80\%$ and $FA^{min}=10\%$ was guided by compromising sufficient low $NDVI$ grid cells for statistical evaluation and reasonable peculiarity of the low $NDVI$ events, which represent a form of extreme event. Furthermore, the main results of this study demonstrate a very low sensitivity to variation in these two threshold parameters, as to a reduction in $n^{min}_{t,ev}$. A substantial change of the identified low $NDVI$ grid cells results only when increasing $n^{min}_{t,ev}$ to five, i.e., almost uninterruptedly negative $NDVI$ in JJA. While these most extreme events would be worth studying, a robust statistical evaluation thereof would not be possible as the number of low $NDVI$ grid cells diminishes drastically (by almost a factor of ten).

2.4 ERA5 reanalysis data

Atmospheric fields are used from ERA5 ~~reanalyses~~ reanalysis from the European Centre for Medium-Range Weather Forecasts (ECMWF, Hersbach et al., 2020) available hourly on 137 vertical levels and ~~interpolated to~~ on a regular grid with 0.5° horizontal resolution.

2.4.1 ~~Seasonal 2-m temperature and precipitation~~Normalized meteorological 90-day anomalies

Our analyses ~~focuses on seasonal averages~~ focus on 90-day mean values of 2-m temperature ($T2m_{90d}$)~~and~~, total precipitation (P_{90d})~~for the periods Sep–Nov (SON), Dec–Feb (DJF), Mar–May (MAM) ,~~, cyclone frequency ($f_{90d}(C)$), and anticyclone frequency ($f_{90d}(A)$). The standard ERA5 variables $T2m_{90d}$ and ~~Jun–Aug (JJA) . For consistency - as we also use moving seasonal (90-day) averages - we calculate seasonal mean values always over 90 days,~~ P_{90d} can directly be averaged, while cyclones and anticyclones are first identified from hourly sea level pressure (SLP) fields. These two most central weather systems are of interest to the low $NDVI$ events' meteorological history as they not only determine vertical and horizontal atmospheric transport of heat, momentum, and moisture, but are further of great importance to the temperature and humidity structure of the atmosphere. Cyclones (anticyclones) are identified according to Wernli and Schwierz (2006) and Sprenger et al. (2017) as objects of low (high) SLP and are, hence, identified from the outermost closed SLP isoline around local SLP minima (maxima). From these hourly object masks we then calculate weather system frequencies over ninety days, i.e., $f_{90d}(C)$ and $f_{90d}(A)$. For all four variables, we calculate 90-day mean values as a right-aligned ~~at the last day of the season~~moving average. Each 90-day mean value, therefore, is labelled by the time step of the last value that contributes to the average. Leap days are discarded from the analysis. The ~~respective climatologies cover SON 1999 to JJA 2020. Throughout the study, we calculate at every grid cell normalized anomalies denoted as $T2m'_{90d}$ and P'_{90d}, e.g.,~~ climatologies of the four variables cover 90-day averages from 1 September 2001 to 31 August 2022.

Based on these 90-day mean values, we compute normalized anomalies at every forest grid cell for variables $X = T2m_{90d}$, P_{90d}, $f_{90d}(C)$, and $f_{90d}(A)$ as follows:

$$\cancel{P}X'_{90d} = \cancel{\frac{P_{90d} - \overline{P_{90d}}}{\sigma_{P_{90d}}}}\frac{X_{90d} - \overline{X_{90d}}}{\sigma_{X_{90d}}} \tag{5}$$

where ~~$\overline{P_{90d}}$ and $\sigma_{P_{90d}}$~~ X'_{90d} denotes the normalized anomaly, $\overline{X_{90d}}$ and $\sigma_{X_{90d}}$ denote the climatological seasonal mean and standard deviation in the considered 21 years, respectively. ~~Note that as for $NDVI'$ (Sect. 2.3), normalization of P'_{90d} and $T2m'_{90d}$~~, i.e., are calculated over 21 values. Note that the normalization of X_{90d} anomalies is used merely for scaling ~~and spatiotemporal comparison , not~~ with local variability. The scaling enables the spatiotemporal comparison of these anomalies and is not used to estimate the ~~values~~anomalies' return period or likelihood.

For better interpretability of individual meteorological histories, we express $f_{90d}(C)$, and $f_{90d}(A)$ also as anomalies relative to the climatological mean. These relative anomalies are calculated as follows, e.g.,:

2.4.2 ~~($T2m'_{90d}$, P'_{90d}) phase space~~

$$f'^{rel}_{90d}(C) = \frac{f_{90d}(C) - \overline{f_{90d}(C)}}{\overline{f_{90d}(C)}} \tag{6}$$

~~Moreover, we characterize the meteorological storylines in the ($T2m'_{90d}$, P'_{90d}) phase space, which we divide into five compartments (see dashed lines in Fig. ??). Q0 denotes the central area within a circle of radius 1 and indicates weak seasonal mean anomalies . Outside this circle, the remaining four compartments correspond to the quadrants of the phase space. We label them clockwise as Q1 (warm-wet), Q2 (hot-dry), Q3 (cold-dry), and Q4 (cold-wet). The frequency of a phase space compartment Q in a given set of events is termed $f(Q)$. The climatological distributions of ($T2m'_{90d}$, P'_{90d}) over all forest grid cells in both biomes and all seasons are shown in Fig. ??. In both biomes and all seasons, $f(Q0)$ is about 40%. $T2m'_{90d}$ and P'_{90d} are anti-correlated in MAM, JJA, and SON (Fig. ??a,c,d,e,g,h), meaning that hot-dry and cold-wet conditions occur more frequently than warm-wet and cold-dry.In the temperate (Mediterranean) biome in JJA, $f(Q2 \vee Q4) = 44.0\%$ (40.8%), while Q1 and Q3 only make up for 14.9% (18.4%) of the season. In contrast, DJF seasonal anomalies are weakly positively correlated in both biomes (Fig. ??b,f), and are, therefore, more often in Q1 or Q3 compared to the other seasons.~~

~~2D hexagonal binning of the climatological frequency distribution of ($T2m'_{90d}$, P'_{90d}) in (a,e) SON, (b,f) DJF, (c,g) MAM, and (d,h) JJA for the (a-d) temperate ($n = 29127$), and (e-h) Mediterranean biome ($n = 7203$), respectively. Dashed lines mark the division into the phase space compartments Q0–Q4, and numbers indicate their climatological frequency~~

2.4.2 Significance assessment

We conduct ~~two similar types of bootstrapping tests to assess significant differences in the meteorological storylines. Both tests~~ a bootstrapping test to identify statistically significant meteorological precursors that are shared among the low $NDVI$ grid cells. The details of how the test is conducted are described in ~~greater detail in~~ Appendix B. Broadly, the bootstrapping produces ~~10~~1'000 synthetic samples of ~~low $NDVI$ events~~ meteorological histories with a sample size equal to the number of low $NDVI$ ~~events under consideration, and we use a significance level of $\alpha = 5\%$. In Sects. 3.3.1, 3.3.2 & ?? we test the~~ grid cells under consideration. These samples correspond to many realizations of meteorological histories that are expected in the climatological reference period of 2002–2022, and are used to construct the null distributions for our statistical tests. We test the following null hypothesis $H_{0,EV}$ at different time lags Δt prior to the event time t_{ev} with a significance level of $\alpha = 5\%$:

> $H_{0,EV}$: The meteorological ~~storyline at $t_0 - \Delta t$~~ history at $t_{ev} - \Delta t$ is unrelated to the occurrence of low $NDVI$ events at ~~t_0~~t_{ev}.

We use different test statistics ~~to investigate several measures~~ (with corresponding null distributions) to investigate different aspects of the meteorological ~~storyline. These measures are the event~~ history under consideration. These statistics are the sample mean $T2m'_{90d}$ ~~and~~ , P'_{90d}, ~~respectively,~~ $f'_{90d}(C)$ and $f'_{90d}(A)$, respectively, and the fraction of Δt that is on average covered by warm ($T2m'_{90d} > 0$) and dry periods ~~, respectively, and the occurrence frequency of each $(T2m'_{90d}, P'_{90d})$ phase space compartment Q per event set~~($P'_{90d} < 0$), respectively. Moreover, ~~the re-sampling~~ our statistical procedure is designed to retain the spatial correlation of the original ~~$T2m$ and P~~ meteorological fields (for details see Appendix B). ~~The median over all 10~~In the bootstrapping test, p-values are estimated from the percentiles of the 1'000 ~~synthetic measures of the meteorological storyline is referred to as the reference climatology $\overline{T2m'^{r}_{90d}}$, $\overline{P'^{r}_{90d}}$, or $\overline{f(Q^r)}$. The reference confidence interval is computed from the 2.5^{th} and 97.5^{th}~~ reference values. Values of the meteorological history under consideration that lie outside the range of the 1'000 corresponding synthetic values of the reference meteorological histories receive a p-value of 0 (Röthlisberger et al., 2016). We reject the above null hypothesis if an observed value lies outside the 2.5$^{\text{th}}$ to 97.5$^{\text{th}}$ percentile of ~~all 10~~the null distribution (defined by the 1'000 ~~values. At time lags~~ values obtained from the bootstrapping). That is, we reject the null hypothesis at the 5% significance level. At time lags Δt ~~when the meteorological storyline of the events lies outside the confidence interval,~~ when the meteorological history of the low $NDVI$ grid cells lies outside the confidence interval, $H_{0,EV}$ is rejected for time lag Δt.

~~In Sect. ?? we employ an analogous technique to identify statistically significant differences in the meteorological storylines of single low $NDVI$ events (EV10) and sequences of events (EV11). Specifically, we draw 10'000 times a sample of n_{EV11} from the meteorological storylines of EV10, where n_{EV11} is the number of EV11. We again receive a 95% confidence interval - this time for the EV10 reference - and thereby test the null hypothesis $H_{0,EV11}$:~~

> ~~$H_{0,EV11}$: The meteorological storyline of EV11 at Δt is the same as that of EV10.~~

2.4.3 ~~Weather systems~~

~~Cyclones and anticyclones are identified from the outermost closed sea level pressure (SLP) contour around local SLP minima and maxima, respectively, according to Wernli and Schwierz (2006) and Sprenger et al. (2017). We calculate seasonal cyclone and anticyclone frequencies, $f_{90d}(C)$ and $f_{90d}(A)$, respectively, as right-aligned averages over 90 days. Moreover, we evaluate $T2m'_{90d}$, P'_{90d}, $f_{90d}(C)$, and $f_{90d}(A)$ continuously over time, i.e., moving 90-day averages.~~

2.5 ~~Forest disturbances~~

~~For evaluating our set of low $NDVI$ events we use the forest disturbance data set by Senf and Seidl (2021a) with an original resolution of 30 m. It is based on a time-series segmentation approach called LandTrendr (Kennedy et al., 2010) and identifies tree canopy mortality. The approach uses two spectral bands (shortwave infrared I and II) and two spectral indices (tasselled cap wetness and normalized burn ratio) from Tier 1 Landsat 4, 5, 7, and 8 images in Jun–Sep. For more details see Senf and Seidl (2021a). From this data set we use the annual disturbance area $D_{J,n}$, which is aggregated for every forest grid cell. D isshown for some exemplary years in Fig. ??. More specifically, we use two measures: the disturbance anomaly D', and the rank of D among the 21 annual values $DR_{J,n}$:~~

$$D'_{J,n} = \frac{D_{J,n}}{\overline{D_J}} - 1$$

$$DR_{J,n} = rank(D_{J,n})$$

~~at forest grid cell J in year n, with $\overline{D_J}$ denoting the climatological mean disturbance area in 2000–2020. The disturbance data overlaps with 73% of the forest grid cells (Fig. 1a), which include 81% of all low $NDVI$ events.~~

3 Results

3.1 ~~Reduced forest performance~~Low $NDVI$ events in JJA 2002–2022

3.1.1 ~~Low $NDVI$ events in 2000–2020~~

Low $NDVI$ events ~~cover~~ covered substantial parts of both biomes in ~~2000–2020~~ JJA 2002–2022, and were by far the most frequent in 2022 (Fig. 2a,d). In the temperate biome, the years with ~~the most wide-spread event coverage~~ most low $NDVI$ grid cells - in descending order - were ~~2018, 2020,~~ 2022, 2019, ~~2003, and 2010~~ 2018, and 2020 (Fig. 2a,d). ~~In 2018 close to 20~~Noteworthy, these four years all lie in the last five years of the study period. In 2022, 37% of temperate forests were affected by ~~reduced greenness, while the two subsequent years covered 11–14% of which large parts were already affected in~~ the low $NDVI$ event, which far exceeded the previous record years 2019 and 2018 by 13% and 15%, respectively (Fig. 2d). ~~Additionally, parts of France and eastern Europe that were unaffected by any event in 2018 experienced some events in the succeeding summers. The top five~~ The top years in terms of affected forest ~~area~~ grid cells in the Mediterranean biome were ~~2017, 2012, 2000, 2001, and 2006~~2022, 2008, 2005, and 2007, again sorted by decreasing area affected. ~~In the most extensive event year 2017, low greenness affected 16% of the Mediterranean forest area~~ Low $NDVI$ grid cells were on average almost twice as frequent in the Mediterranean biome (9% yr^{-1}) compared to the temperate biome (5% yr^{-1}; Fig. 2d). Lastly, most low $NDVI$ events in each biome go along with increased disturbance area as measured by forest canopy mortality according to Senf and Seidl (2021a, Appendix C). More specifically, in the overlap period of the two data sets, most low $NDVI$ grid cells

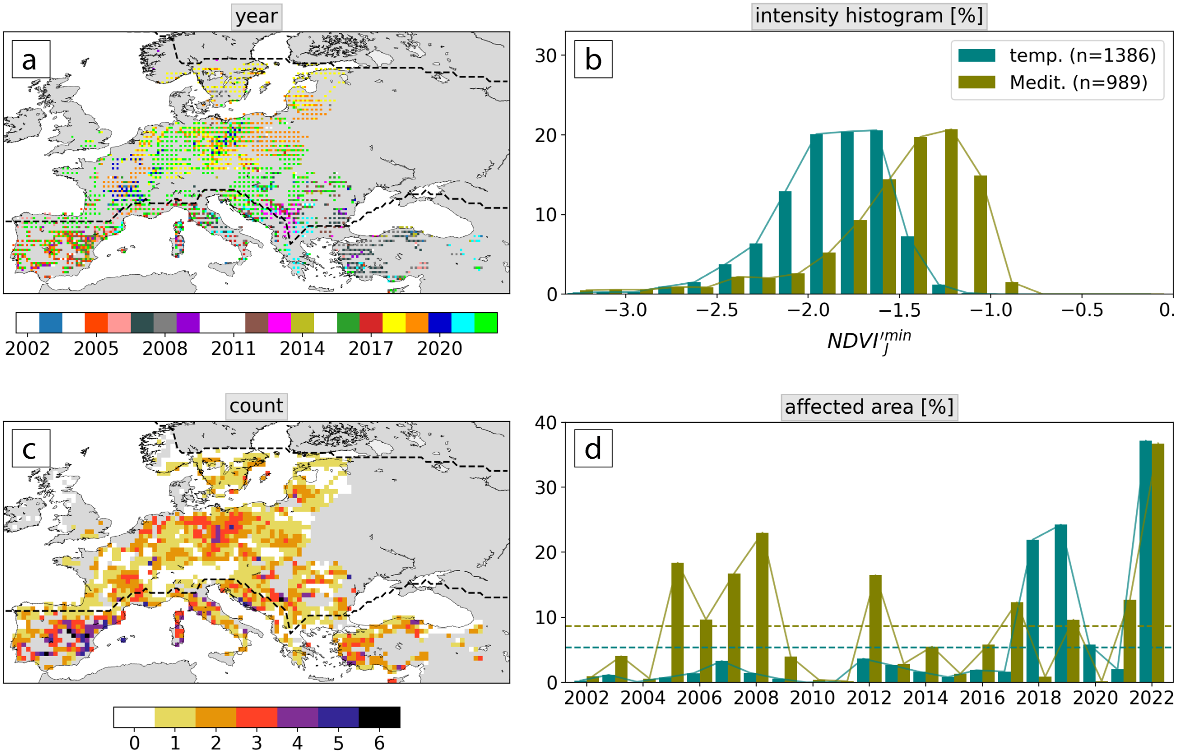

Figure 2. Maps of (a) years with a low $NDVI$ event~~year~~, and (c) total number of events. (b) Histogram of event intensity as measured by ~~$NDVI'^{min}$, (c)~~ $NDVI'^{min}_J$ in the ~~number of events per forest grid cell~~two biomes, and (d) time series of the ~~event-affected forest~~ biome-integrated area of low $NDVI$ grid cells relative to ~~the total temperate and Mediterranean biome~~ all forest grid cells (in %). Years with ~~less than 15 events~~ few low $NDVI$ grid cells are shown in white in (a). In (a) ~~and (b)~~ each grid cell is split into four quads, ~~therefore~~ showing the ~~variables for~~ event year of up to the four most intense events. Dashed lines in ~~different~~ (d) show the average over all years. Dashed lines in (a,~~ordered by intensity from top left to bottom right~~c) delineate the temperate and Mediterranean biome.

are among the top four and five ranks regarding the disturbance area in temperate and Mediterranean forests, respectively.

~~Furthermore, the intensity and frequency of the low $NDVI$ events varied over Europe.~~Mediterranean forests faced more but typically less intense events, as measured by the grid cell-wide average of summer minimum $NDVI'$ (Fig. 2b, Sect. 2.3). $NDVI'^{min}_J$ was usually between -1 and -2 IQRs, whereas it was about 0.5 lower for temperate forests. Hot-spot regions with ~~two to three~~ three or more events during the 21 years were ~~Germany, France, and southeastern Europe~~ northeastern Germany, the Balkans, and large parts of the Mediterranean biome (Fig. 2c). ~~The latterwas affected mainly in 2000,~~ In the latter, we find many low $NDVI$ grid cells in Spain in 2005, in Turkey in 2007 ~~,~~ and ~~in 2012–2013~~2008, in Italy in 2017, and in 2022 in the northern Mediterranean (Appendix D). Central Europe was largely affected ~~by the 2018–2019 events, while further to the Southwest, 2003, 2005–2006, 2015, and 2019–2020 were the most dominant event years (Fig. 2d). Event intensity as measured~~

~~by $NDVI'^{min}$ (see Sect. 2.3) averaged at −2.7 in both biomes, and was strongest in events in southeastern Europe and~~ in the ~~2010 event in Russia (Fig. 2b). Two forest grid cells in the French Massif Central and one in the UK were struck by four or five events, which, however, were of only intermediate intensity~~past five years, while the 2018–2019 events extended further to Scandinavia and the Baltic, and 2020 and 2022 affected also parts of southern France and eastern Europe, respectively. Note that ~~one third~~ 26% of the forest regions in the study domain never experienced an event in JJA ~~2000–2020~~ 2002–2022 (Fig. 2c). These grid cells are in northeastern Europe or in mountainous regions including the Alps, the Carpathians, the southern Dinaric Alps, and the Eastern Black Sea Mountains. ~~After a brief comparison of low $NDVI$ events to independent forest disturbance data in the following section, we use these events in both biomes separately as the basis for specific meteorological analyses in Sect. 3.3.~~

3.1.1 ~~Event evaluation~~

3.2 Examples of meteorological histories

~~To evaluate the low~~ Low $NDVI$ events ~~identified in the previous sections, we qualitatively compare them to the independent disturbance data set of Senf and Seidl (2021a). In 67% of all~~ affected different forest regions all over Europe with varying intensity, each with its own meteorological history. We first present three examples of low $NDVI$ events ~~the disturbance area D is larger than on average in 2000–2020 - more often in the temperate (69%)than in the Mediterranean biome (56%~~that affected regions in Spain in 2005 (SPA05), in the Balkans in 2013 (BAL13), and in France in 2022 (FRA22; Fig. ~~C1a,c). The median disturbed area increases by +23% and +13% during events in the temperate and Mediterranean biome, respectively.Furthermore, non-events typically go along with negative D' in the temperate (64% of non-events) and the Mediterranean biome (66%).Figure C1b,daddit shows the disturbance area rank, DR, from~~ 3). First, these examples illustrate that the low $NDVI$ events identified in this study not necessarily featured a very low $NDVI_J'^{min}$, i.e., a strong magnitude of negative $NDVI'$. For example, some grid cells of the SPA05 region were identified as low $NDVI$ grid cells with $NDVI_J'^{min}$ just above -1~~(smallest D in 2000–2020)to 21 (largest D). With 1–5 events per affected forest grid cell (Fig. 2)an event would go along with DR 17–21 if the event years were equal to the years of largest disturbed area. Most events indeed cover ranks 17–21 and 16–21 for the temperate and Mediterranean biome, respectively. We conclude that~~, while others with $NDVI_J'^{min} < -1.75$ in northern Spain were not identified (Fig. 3a,d). In fact, this is an expected behaviour of our identification scheme as low $NDVI$ grid cells are meant to indicate that a very large fraction of forest pixels in that grid cell experienced persistently low $NDVI$ (Sect. 2.3). In many cases, however, event intensity as a JJA-integrated quantity is in many cases increased at low $NDVI$ ~~events tend to go along with more forest disturbances, i.e. , enhanced canopy mortality, and rank among the largest forest disturbances at forest grid cells~~ grid cells, compared to their event-unaffected surrounding, illustrated at the example of France in 2022 (Fig. 3c,f). Lastly, another interesting case (not shown) occurred in 2014 in Slovenia, where an ice storm in DJF-6m caused a few low $NDVI$ grid cells (Appendix D; Buras et al., 2021; Senf and Seidl, 2021c).

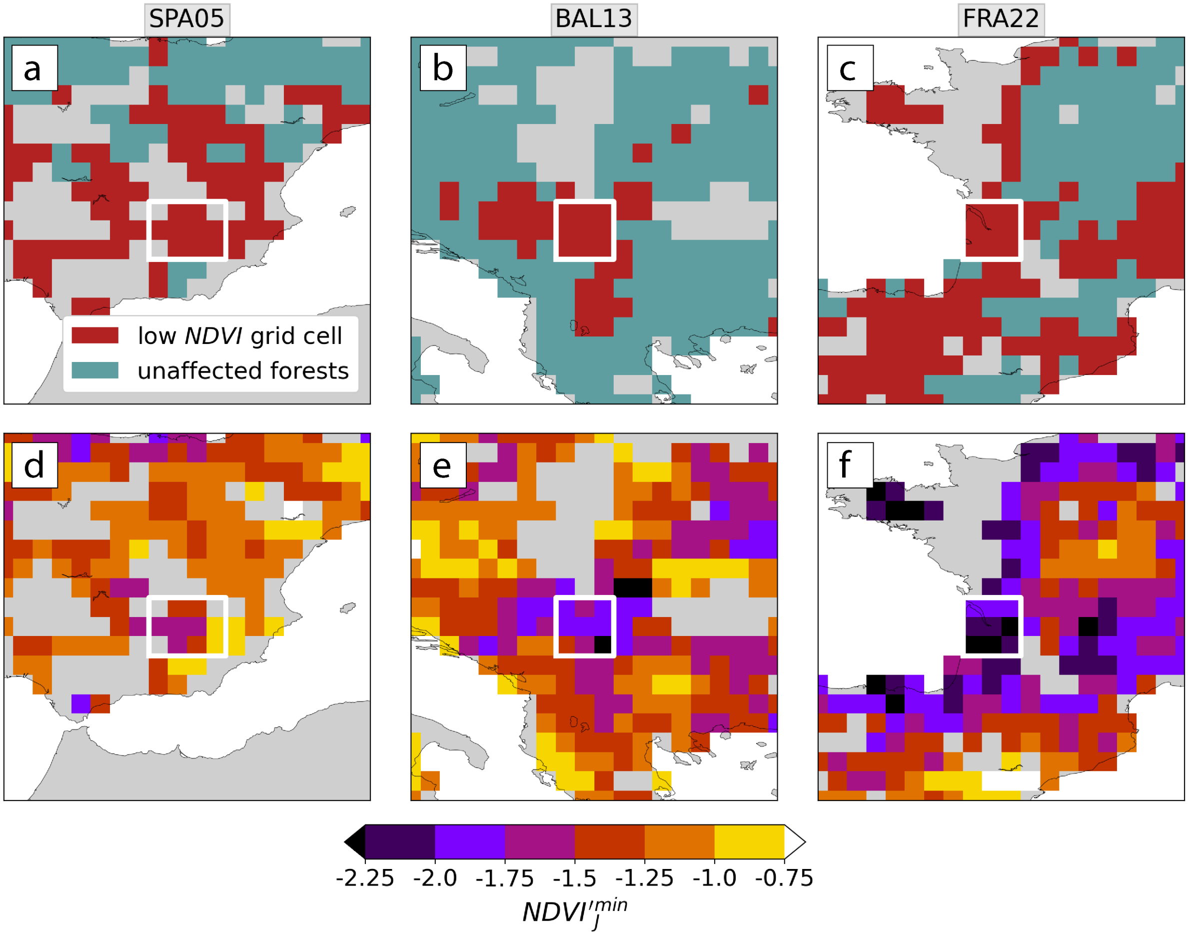

Figure 3. ~~Event evaluation for~~ (~~a,b~~a-c) ~~the temperate~~ Low $NDVI$ grid cells and (~~c,d~~d-f) the ~~Mediterranean biome.~~ event intensity measured by $NDVI'^{min}_J$ in (a,~~c~~d) ~~box plots of the disturbance anomaly D' of low $NDVI$ event~~ Spain in 2005, (~~red~~b,e) ~~and non-event grid cells~~ the Balkans in 2013, (~~turquoise~~c,f) ~~.~~ France in 2022. The ~~distribution mean is shown by a yellow triangle~~focus regions of SPA05, ~~outliers~~ BAL13, and FRA22 are ~~omitted~~framed with white boxes.~~(b,d) histograms of ranks 1–21 of disturbance area DR of low $NDVI$ event grid cells. The median is shown by the vertical line.~~

~~While the two data sets correspond particularly well in years of widespread events , e. g., 2003, 2018, 2019, and 2020 (see~~ We now introduce the concept of a three-year meteorological history prior to low $NDVI$ events for these three examples. For SPA05, the meteorological history was characterized by a shift from a precipitation surplus during SON-21m to JJA-12m to a precipitation deficit during the year prior to the low $NDVI$ event (Fig. ~~??), there are substantial discrepancies between the two data sets in other years. For example, 36% of non-event grid cells experience a positive D'.We show in Appendix ??~~ ~~that several severe winter storms caused large D but did not manifest in very low $NDVI$ in the following summer.Examples for storms that were not followed by a~~ 4a). Note that we here use a notation for seasons (e.g., SON-21m) that indicates their negative time lag to the events (i.e., SON-21m is the autumn 21 months prior to the low $NDVI$ event ~~are Lothar in western Europe in winter 1999/2000, Gudrun in Scandinavia in 2004/05, Kyrill in Germany in 2006/07, and Vaia in northern Italy in 2018/19. Furthermore, D of several low $NDVI$ events ranks among the lowest during the study period, which can be explained by a number of conceptual, technical, and physical reasons (see discussion in Sect. 4.1). Nevertheless, Fig. C1 reveals that low $NDVI$ events are also associated with increased canopy mortality and we, thus, proceed to analyzing their meteorological storyline.~~

3.3 ~~Meteorological storyline of low $NDVI$ events~~

~~We investigate four characteristics of the meteorological storyline prior to low $NDVI$ events separately for the two biomes.Thereby, we first consider the anomalies $T2m'_{90d}$ and P'_{90d} and their link to anomalous weather system frequencies continuously (~~summer, termed JJA-ev). While the cyclone frequency was more than doubled during the former wet period, the period with negative P'_{90d} featured almost no cyclones at all. The relative cyclone frequency anomaly $f'^{rel}_{90d}(C)$ was most negative (-50% to -100%) in the climatological cyclone season from SON to MAM (Fig. 4a). For example in early MAM-3m, $P'_{90d} = -1.5$ coincided with $f'^{rel}_{90d}(C)$ of close to -75%. The meteorological history of SPA05 further featured strong cold spells in MAM-15m to JJA-12m and in DJF-6m to MAM-3m with $T2m'_{90d}$ as low as -2.6 (Fig. 4b). Warm periods occurred in JJA-ev and DJF-18m and coincided with an increased frequency of anticyclones, i.e., ~~a right-aligned 90-day running mean)~~ positive $f'^{rel}_{90d}(A)$. In the second example, BAL13, the magnitude of negative P'_{90d} was also a dominant feature of the meteorological history with even more distinctive persistence over the three years ~~prior to the events (Sect. 3.3.1). Second, we assess the persistence of these anomalies (Sect. 3.3.2). Based on these results, we focus on the shorter meteorological storyline of the six previous seasons to, thirdly, compare the meteorological storyline of event sequences (i.e., two consecutive summers with~~ (Fig. 4c). Similar to SPA05, a precipitation deficit was often related to negative $f'^{rel}_{90d}(C)$ with some exceptions, e.g., in SON-9m. JJA-12m was characterized by the largest $T2m'_{90d} = +2.9$ of all examples and neither coincided with substantial changes in $f'^{rel}_{90d}(A)$ or in $f'^{rel}_{90d}(C)$ (Fig. 4c,d). Despite continuously positive $T2m'_{90d}$ from JJA-12m to JJA-ev, the meteorological conditions became less dry and less hot than in JJA-12m, when, interestingly, the BAL13 region was mostly unaffected by low $NDVI$ events ~~) with those of single events (Sect. ??). Lastly in Sect. ??, we analyze anomalies in the frequency of seasonal ($T2m'_{90d}, P'_{90d}$) phase space compartments, again addressing the link to weather systems.~~(Appendix D). The most recent event FRA22 had again a different meteorological history. It stands out with anomalously high $T2m'_{90d}$ over the six months preceding the event that was related to negative $f'^{rel}_{90d}(A)$ over considerable portions of that period (Fig. 4f). Moreover, P'_{90d} during most of these six months was only slightly negative, and strongly positive when going further back in the meteorological history, e.g., in JJA-12m (+2.6; Fig. 4e). One last noteworthy disparity of FRA22 compared to BAL13 is that JJA-12m was persistently colder alongside negative $f'^{rel}_{90d}(A)$.

3.2.1 ~~Uni-variate P'_{90d} and $T2m'_{90d}$ and weather system frequencies~~

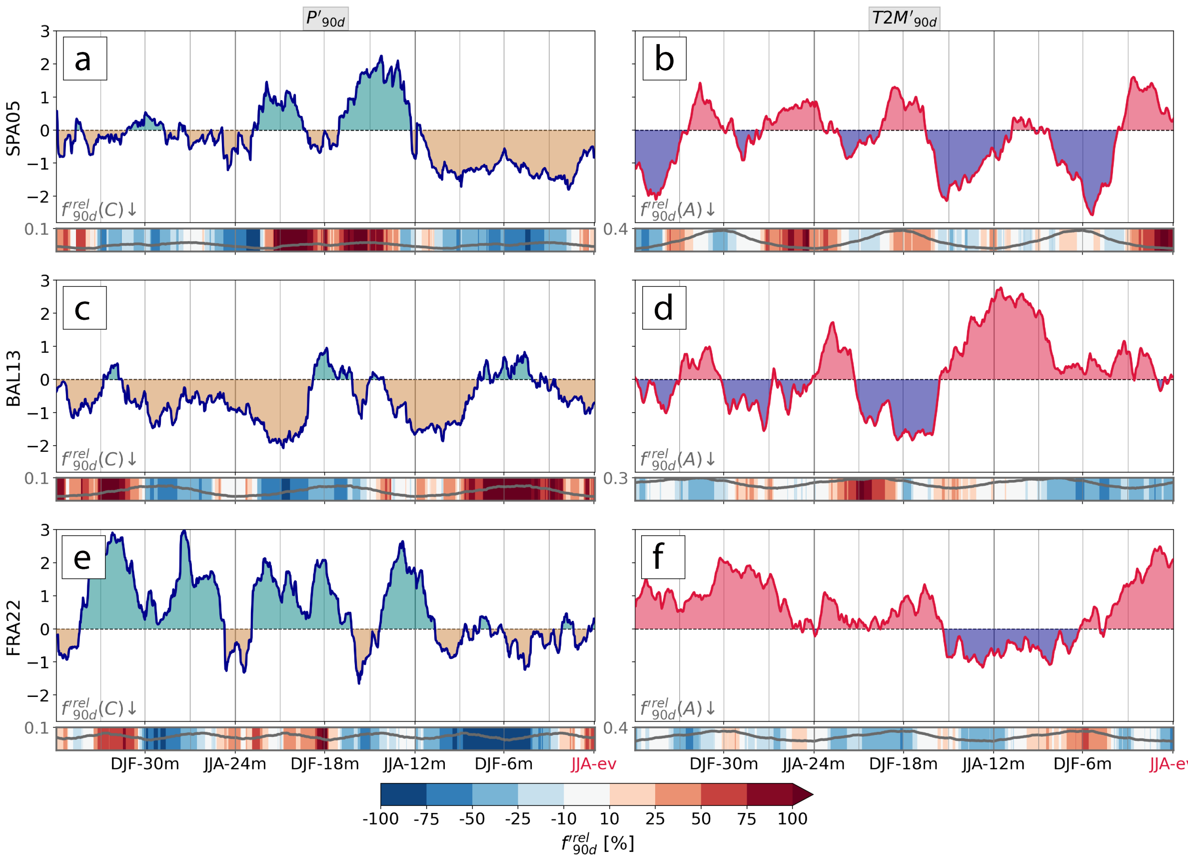

Figure 4. ~~Average three-year~~ Three-year evolution of (a,c,e) P'_{90d} and (b,d,f) $T2m'_{90d}$ leading up to low $NDVI$ events in (~~red lines~~a,b) ~~. The grey shading displays the confidence interval of the tested null hypothesis $H_{0,EV}$~~ Spain in 2005, ~~i.e., the $2.5^{th} - 97.5^{th}$ percentile of the reference climatology~~ (~~see Sect. 2.4.2~~c,d) ~~. Solid and dashed lines show~~ the ~~90-day~~ Balkans in 2013, (e,f) ~~cyclone and (g,h) anticyclone frequency~~ France in ~~climatology and during events, respectively. Colored shading indicates the respective anomalies $f'_{90d}(C)$ and $f'_{90d}(A)$. Plots apply to events in the~~ 2022. The relative anomaly of (a,c,e~~,g~~) ~~temperate~~cyclone frequency, and of (b,d,f~~,h~~) ~~Mediterranean biome~~anticyclone frequency is shaded and their climatological mean is shown as grey line in the heat map panels.

~~Figure 5 displays the evolution of P'_{90d} and $T2m'_{90d}$ and collocated weather system frequencies for eventsin both biomes. For instance, the red line in Fig. 5a shows the time evolution of the 90-day averaged precipitation anomaly during the three years~~ While they are illustrative, these exemplary meteorological histories of SPA05, BAL13, and FRA22 reveal great variability and clearly do not allow to draw any causal inferences about how certain aspects of these histories alter the likelihood of low $NDVI$ events. The events' meteorological histories share certain characteristics but also clear disparities emerge, for example, P'_{90d} in JJA-ev or $T2m'_{90d}$ in the last year before the event. In the next section we thus systematically analyze the meteorological history of all identified low $NDVI$ events, and use our sub-sampling and bootstrapping procedure to identify statistically significant meteorological precursors to these events. Again recall that these precursors are features of the low $NDVI$ events' meteorological histories that were statistically significantly more frequent prior to low $NDVI$ events ~~, averaged for all 1'228~~ compared to climatology.

3.3 Systematic meteorological precursors of low $NDVI$ events

The previous two sections have illustrated that (i) low $NDVI$ events were unequally distributed over the study period - especially in temperate forests -, and (ii) a more systematic analysis of meteorological histories is needed to assess their relevance for the low $NDVI$ ~~events~~ grid cells. To account for the uneven distribution of events across years, we investigate the average meteorological history of a random sub-sample of low $NDVI$ grid cells in the temperate ~~biome. The events occur in JJA-0m on the very right of the diagram and are characterized by a precipitation deficit of about 1 standard deviation. This is clearly outside of the confidence interval of the hypothesis test that evaluates $H_{0,EV}$: "The meteorological storyline is not related to the occurrence of~~ and Mediterranean biome separately. The sub-sample includes a maximum of ten randomly selected low $NDVI$ grid cells per year. Given the 21-year-long study period, there is a maximum of 210 contributing low $NDVI$ grid cells. For years with less than or exactly ten low $NDVI$ grid cells, all events of the respective year contribute to the sub-sample. The resulting average meteorological history of the temperate and Mediterranean biome is a mean over 170 and 164 low $NDVI$ grid cells, respectively (see Appendix A). Due to the randomness involved in the sub-sampling, we repeat the procedure $n_{samp} = 10$ times to create a variety of average meteorological histories that account for the variability in years when many low $NDVI$ grid cells were identified. Our bootstrapping test (significance level $\alpha = 5\%$) is then applied to the anomalies of the averaged meteorological histories to identify statistically significant meteorological precursors of the low $NDVI$ events ~~"~~ in 2002–2022 (Sect. 2.4.2).

~~First of all, event anomalies more than two years back (before JJA-24m) are mostly within the reference confidence interval, i.e., are not significantly different from the climatological reference. After that, periods of negative P'_{90d} are highly prominent in both biomes (~~In the first part of this section, we analyse the magnitude of $T2m'_{90d}$, P'_{90d}, $f'_{90d}(C)$, and $f'_{90d}(A)$ during the three years leading to low $NDVI$ events - similar to Fig. ~~5a, b) . In~~ 4. Second, we investigate the persistence of dry ($P'_{90d} < 0$) and hot ($T2m'_{90d} > 0$) meteorological anomalies.

3.3.1 Magnitude of meteorological anomalies

The most remarkable meteorological precursors of low $NDVI$ events in the temperate biome ~~, a first period of~~ are significantly negative P'_{90d} ~~stretches over almost the entire year prior to events , and is significant at DJF-18m and MAM-15m (~~and positive $T2m'_{90d}$ during the four months preceding the events (bold lines in Fig. 5a~~). Interestingly, DJF-6m is wetter than usual with a peak anomaly of +0.4 that is significantly different from the reference climatology. Afterwards, P'_{90d} drops abruptly and is significantly reduced in~~ ,c). Note that the 90-day anomaly four months prior to ~~events, reaching −1.0 during JJA-0m. In the Mediterranean biome during twenty~~ the event represents the conditions during the six to four months prior to ~~events,~~ JJA-ev, i.e., the time instances denoted here and in the following mark the end of the anomalous time periods. Furthermore, the meteorological history of low $NDVI$ events in temperate forests showed significantly reduced P'_{90d} in JJA-12m (Fig. 5a).

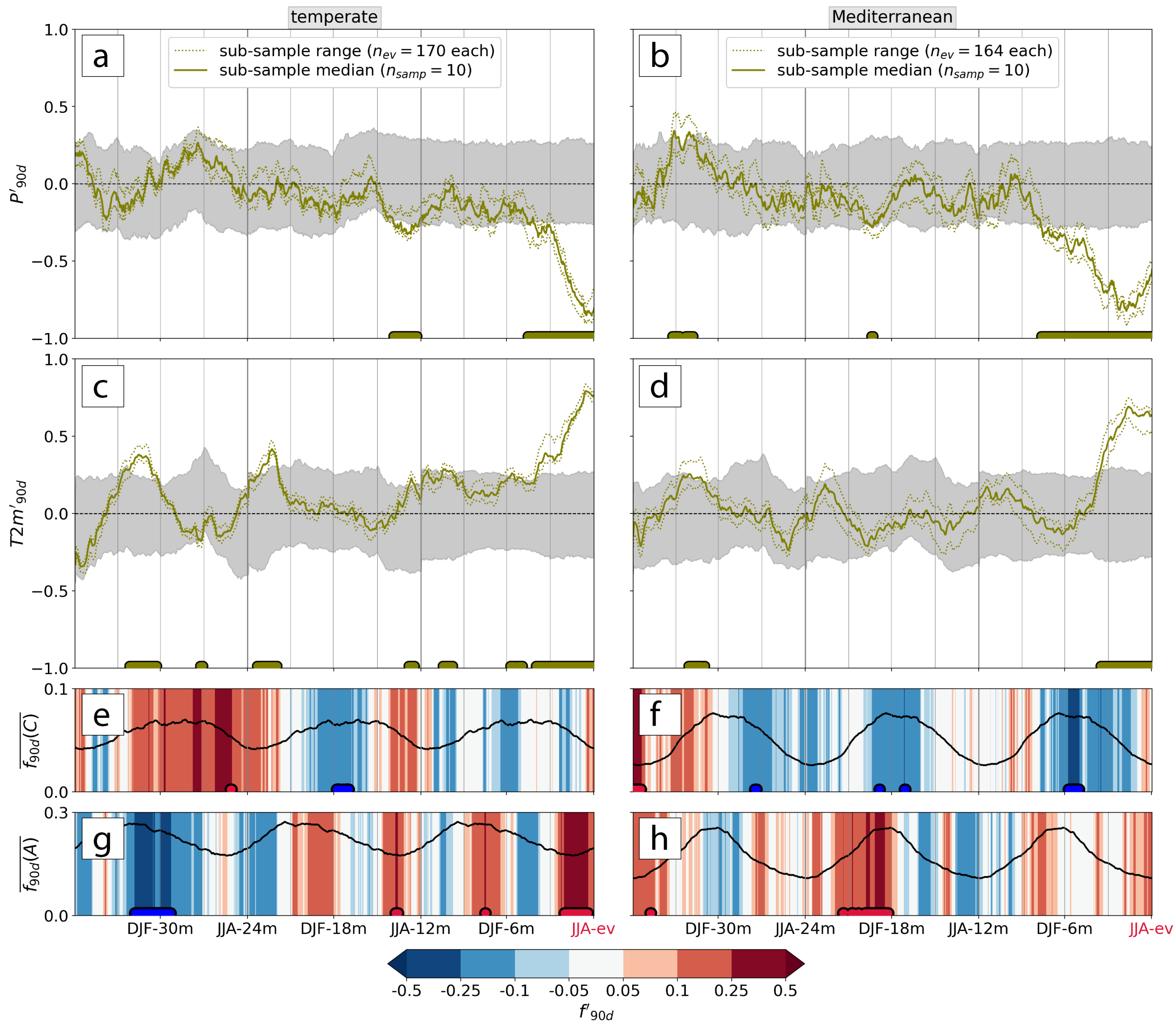

Figure 5. Average three-year evolution of (a,c) P'_{90d} and (b,d) $T2m'_{90d}$ at low $NDVI$ grid cells (olive lines). The range spanned up by the $n_{samp} = 10$ sub-samples (of n_{ev} low $NDVI$ grid cells each) is dotted, their median in solid. The confidence interval (CI), i.e., the $2.5^{th} - 97.5^{th}$ percentile of the reference climatology is shaded grey (see Sect. 2.4.2). The normalized (e,f) cyclone and (g,h) anticyclone frequency anomalies $f'_{90d}(C)$ and $f'_{90d}(A)$, respectively, as median over the 10 samples are shaded in colors. The 90-day climatology of the weather system frequencies is displayed as solid line. Plots apply to events in the (a,c,e,g) temperate, and (b,d,f,h) Mediterranean biome. Statistically significant median values outside the 95% CI are marked by colored dots at the bottom of each panel.

In between JJA-12m and JJA-ev, P'_{90d} ~~is continuously negative and exerts distinct significant peak values (Fig. 5b).The $H_{0,EV}$ can further be rejected for P'_{90d} in JJA-0m, when P'_{90d} drops to about -1.0. All in all, distinct features of the events' previous P'_{90d} evolution are a dry JJA-0m, negative P'_{90d} already in the previous year, and, in the temperate biome, a remarkable wet period in the cold season prior to the events.~~

~~In some contrast~~ remained mostly negative but not with a statistically significant magnitude. Similar to P'_{90d}, ~~after JJA-24m the meteorological storyline in the Mediterranean biome features positive $T2m'_{90d}$ in JJA and negative~~ also for $T2m'_{90d}$ significant signals along the meteorological history were always of the same sign (positive in ~~DJF, although these anomalies are largely not statistically significant~~ the case of $T2m'_{90d}$). Further warm peaks occurred in MAM-3m, in SON-9m, in JJA-12m, in SON-21m, and in DJF-30m (Fig. 5~~d). In the temperate biome, $T2m'_{90d}$ is almost exclusively positive after JJA-24m and is unusually increased during SON-21m and SON-9m~~ c). Many of the highlighted periods when the magnitude of meteorological conditions were unusual coincided with larger spread of the ten low $NDVI$ grid cell sub-samples. For example, P'_{90d} in JJA-12m ranged between $-0{,}2$ and -0.4, indicating that the years with many low $NDVI$ grid cells (e.g., 2022, 2019, and 2018) showed increased variability at that point in time (Fig. 5~~e). The most prominent (and highly significant) warm anomaly of +1.2 and +0.8 arises during the three and four months prior to events in the temperate and Mediterranean biome, respectively~~ a). That is, some $NDVI$ grid cells showed a stronger, and others a weaker or no precipitation deficit in JJA-12m, respectively.

In Mediterranean forests, the magnitude of hot and dry anomalies in JJA-ev were comparable to those in temperate forests, with the difference that significantly negative P'_{90d} emerged already eight months before low $NDVI$ events during DJF-6m (Fig. 5~~e~~b,d). ~~So a hot JJA-0m, and, in~~ One more dry period in DJF-18m was significantly different from climatology, as was a wet and warm anomaly in DJF-30m (Fig. 5b). Apart from the few mentioned anomalies, the ~~temperate biome, warm periods in SON-21m and~~ meteorological anomalies further back than three seasons (before SON-9m~~emerge as key constituents of the meteorological storyline of~~) were within the variability expected from the climatology. Similar to temperate forests, the uncertainty induced by the random sub-sampling is larger when anomalies were of greater magnitude. This applies in particular for the anomalies preceding the low $NDVI$ events by more than one year.

Most of ~~these distinct anomalies relate to a specific collocated weather system frequency anomaly. In Mediterranean forest regions, the climatological peak in 90-day averaged cyclone frequency , $f_{90d}(C)$, of ∼10% occurs from DJF to MAM~~ the highlighted anomalies in surface meteorology went along with significant anomalies in the occurrence frequency of weather systems (Fig. 5~~f). In particular in the 20 month-long dry period, $f_{90d}(C)$ is reduced twice during that peak phase by up to −3%.The onset of that dry period in SON-21m is related to the strongest increase in anticyclone frequency during the entire meteorological storyline of $f'_{90d}(A) = +5\%$~~ e-h). Note that we here explore the median history of $f'_{90d}(C)$ and $f'_{90d}(A)$, i.e., of normalized anomalies that are comparable across space and time, and not of $f'^{rel}_{90d}(C)$ and $f'^{rel}_{90d}(A)$ as in Sect. 3.2, which are more meaningful in a local context (Sect. 2.4). In the temperate biome, the hot-dry conditions leading up to JJA-ev related to a concurrent positive $f'_{90d}(A)$ (Fig. 5~~b,h). Further,~~ g). Already in JJA-12m, negative P'_{90d} went along with significantly increased $f_{90d}(A)$~~is increased at the beginning and during the most intense phase of the significantly drier period from DJF-6m to JJA-0m. Similarly in the temperate biome,~~. These positive anomalies thereby occurred in the season when anticyclones are climatologically the least frequent. Further back in time, negative $f'_{90d}(C)$ in MAM-15m had no direct connection to anomalies in surface meteorology, and the DJF-30m warm anomaly related to persistently negative $f'_{90d}(A)$. In the Mediterranean biome, there were four periods of significantly negative $f'_{90d}(C)$~~co-occurs with the pronounced dry periods from SON-21m to JJA-12m~~

~~and from MAM-3m to JJA-0m~~: two of them, in DJF-18m and during the 8-month long dry period before the event, coincided with $P'_{90d} < 0$ (Fig. 5~~a,e). Positive $f'_{90d}(C)$ only occurs during the intermittent wet period when the anticyclone frequency is reduced by $\sim -2\%$ (note the climatological value of 20–30%;~~ f). Note that these were during periods when cyclones are climatologically the most frequent. Moreover in the drier than usual DJF-18m, $f'_{90d}(A)$ was persistently positive (Fig. 5~~g). As for Mediterranean forests, the three significantly drier periods in temperate forests in DJF-18m, JJA-12m, and JJA-0m correspond to peaks in $f'_{90d}(A)$ of +2 to +5%. The effect of the two weather systems on~~ h). To summarize, significant changes in weather system frequencies often occurred simultaneously with the time periods when the magnitude of P'_{90d} and $T2m'_{90d}$ ~~depends on the season. Anticyclones cause locally warmer conditions in JJA (~~were identified as meteorological precursors of low $NDVI$ grid cells.

The systematic assessment of meteorological histories across all low $NDVI$ grid cells in 2002–2022 has revealed several meteorological precursors of low $NDVI$ events in temperate and Mediterranean forests. In addition to the mere magnitude of $T2m'_{90d}$ and P'_{90d}, some of these anomalies have co-occurred with a significantly altered frequency of cyclones and/or anticyclones. At the biome scale, anticyclones went along with locally drier conditions across all low $NDVI$ grid cells, e.g., in ~~JJA-0m) and colder conditions in DJF (e.g.,~~ JJA-ev and in JJA-12m (temperate), and in DJF-18m ~~), respectively (Fig. 5c, d, g,h). The effect of cyclones on~~ (Mediterranean). Further, the lack of cyclones in the Mediterranean in their climatological peak season linked to significantly reduced P'_{90d}. Figure 5 reveals that some $T2m'_{90d}$ ~~is less systematic at the biome scale (cf.~~ and P'_{90d} signals were not significantly unusual in their magnitude, however, seem to have been of unusual persistence. For example, warm anomalies in temperate forests were hardly ever interrupted during the entire meteorological history (Fig. ~~??)and will be addressed amongst others in Sect. ??. All in all, collocated weather systems seem to have a clear imprint on the most anomalous periods of the meteorological storyline~~5c). Therefore, we next analyze the persistence of dry and warm anomalies.

3.3.2 Persistence of dry and warm periods

~~The percentage of the integration period with a biome-wide average (a,c) dry ($P'_{90d} \leq 0$) and (b,d) warm periods ($T2m'_{90d} \geq 0$) for decreasing integration period Δt prior to low $NDVI$ events. The grey shading displays the 95% confidence interval (CI) of the reference climatology (see Sect. 2.4.2).~~

The previous section ~~also~~ pointed to not necessarily intense but unusually persistent dry and warm periods, which we investigate in more detail in ~~Figure~~Fig. 6. To do so we take the data displayed in Fig. 5 and compute the fraction of positive and negative ~~anomalies of~~ $T2m'_{90d}$ and P'_{90d}, respectively, from a single ~~seasonal~~ 90-day average to three years prior to the low $NDVI$ events~~(red line in Fig. 6)~~. This is done, again, for the ten sub-samples individually, of which we calculate a median time series. Moreover, analogously to Fig. 5, we contrast the respective fractions to values expected under the null hypothesis $H_{0,EV}$ that the fraction of dry~~and~~/warm periods preceding the low $NDVI$ events (i.e., during Δt) ~~are~~ were unrelated to these events (grey shading in Fig. 6; Sect. 2.4.2).

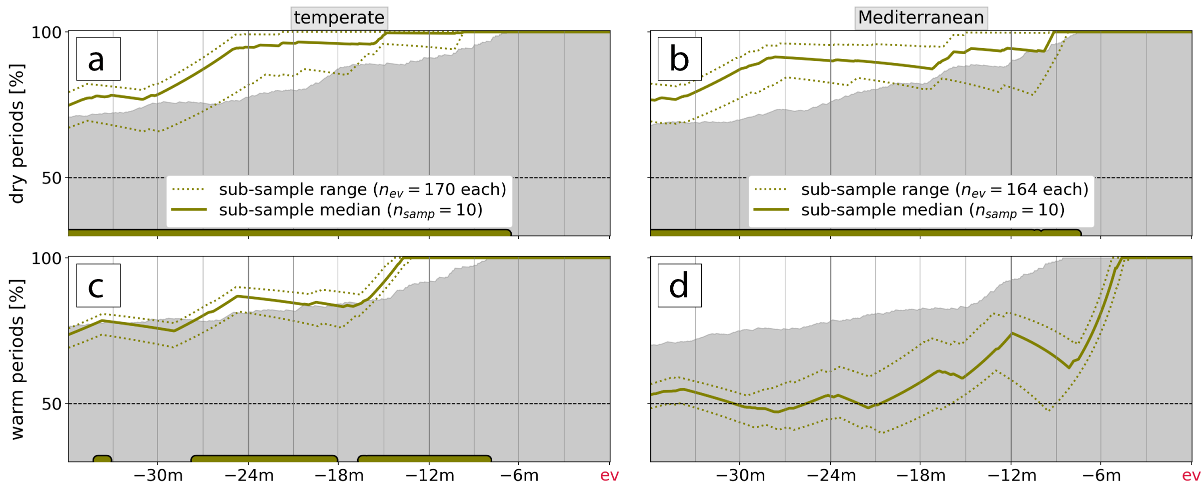

Figure 6. The average fraction of the integration period with a (a,c) dry ($P'_{90d} < 0$) and (b,d) warm period ($T2m'_{90d} > 0$) for decreasing integration period Δt prior to low $NDVI$ events. The range spanned up by the $n_{samp} = 10$ sub-samples (of n_{ev} low $NDVI$ grid cells per biome) is dotted, their median in solid. The grey shading displays the 95% confidence interval (CI) of the reference climatology. Statistically significant median values outside the 95% CI are marked by colored dots at the bottom of each panel.

In the temperate biome, ~~the 5-month persistence of the most recent dry period up to JJA-0m is not unusual~~ when going back more than 8-months prior to low $NDVI$ events, the persistence of warm and dry anomalies was each a statistically significant meteorological precursor to low $NDVI$ grid cells in 2002–2022 (Fig. 6a~~),contrary to its~~ ,c). While $T2m'_{90d}$ and P'_{90d} prior to this period were only shortly of significant magnitude (Fig. 5a~~). However, when~~ ,c), their persistence was unusual farther back along the meteorological history. When considering two years before events, dry periods ~~make up almost 80~~accounted for 82–99% of that time period, where the range is spanned up by the ten random sub-samples, which is significantly ~~different from~~ more than the climatological expectation ~~. Thus, the fact that 80~~(Fig. 6a). Similarly, the persistence of warm anomalies during 81–90% of the preceding two years ~~are anomalously dry emerges as a further key aspect of the meteorological storyline of temperate biome low~~ were significantly anomalous (Fig. 6c) for nine out of the ten sub-sample meteorological histories (not shown). When considering all ten sub-samples separately, we find that the persistence of dry periods and warm periods was significantly different from climatology at least over 26 and 25 months prior to low $NDVI$ ~~events. Warm periods accumulate to a highly unusual degree when integrating over more than ten preceding months , and are interrupted by hardly any cold period (Fig. 6c). This characteristic is~~ events, respectively. This is also the integration period when these two meteorological precursors were most distinct - i.e., ~~most clearly rejects~~ when $H_{0,EV}$ ~~- at a time scale of 18 months before low~~ ~~$NDVI$~~ ~~events. So persistent and recurrent warm anomalies and~~ is most clearly rejected. So an accumulation of both warm and dry periods over the about two previous years ~~are~~ were peculiarities of events in the temperate biome.

In the Mediterranean biome, warm periods ~~are more frequent~~ were more frequent than usual but not significantly so compared to the reference climatology (Fig. 6d), ~~while~~ which is an interesting contrast to the temperate biome. None of the ten sub-samples indicates that positive $T2m'_{90d}$ were unusually persistent for any Δt during the meteorological history. Similar to the temperate biome, dry periods accumulate to a highly unusual degree ~~. When~~ when going back more than eight months ~~, the frequency of dry periods is clearly unique to low $NDVI$ events~~ (Fig. 6b). The lowest p-value is reached ~~20~~ 28 months prior to events, when ~~the uninterrupted dry period starts to arise. So in the Mediterranean, prior to low $NDVI$ events dry periods persist over 18 months and are a distinct feature of the events' meteorological storyline considering time periods up to 31 months prior to the events~~ dry periods persisted over 81–95% of the time afterwards. Again considering each of the 10 sub-samples individually, we conclude that the persistence of dry periods was increased over at least 34 months preceding low $NDVI$ events, which is longer than for low $NDVI$ events in temperate forests. In contrast, the persistence of warm conditions ~~appears not to be crucial for Mediterranean~~ does not emerge as a significant precursor to low $NDVI$ events in the Mediterranean.

3.3.3 ~~Event sequences~~

3.4 Spatial patterns of weather system anomalies

~~In addition~~ Additional to the biome-wide ~~analyses of the previous sections, Figure ?? shows the meteorological storyline of two subgroups: two-year event sequences (EV11) and single events including their recovery (EV10). The two-digit binary code indicates whether there was an event in JJA-0m, and in JJA+12m, respectively. This time, we test the null hypothesis $H_{0,EV11}$ that the meteorological storyline of EV11 is the same as that of EV10 (blue shaded confidence interval in Fig. ??; Sect. 2.4.2). Note that the meteorological storyline of the two subgroups are fairly similar especially for the temperate biome as forest regions belonging to EV10 and EV11 can be neighbouring, and as EV11 mostly occur when EV10 are wide-spread too. The signal of EV10 stems to 42% from 2018/19 and 2019/20 when also 82% of EV11 occur. Nevertheless,~~ averages shown in Fig. 5e-h, anomalies in weather system frequencies exert some typical spatial patterns along the meteorological history, which we illustrate at the example of the ~~differences between the two can be instructive about why a second event occurs in EV11 but not in EV10. Moreover, the meteorological storyline of EV10 up to JJA-0m is very similar to that of all events (Fig. 5), as - due to the grouping - only sequential events ($n = 92$) and those in 2020~~ past year prior to JJA-ev. Based on our set of low $NDVI$ grid cells, we identify common patterns in the anomalies of weather system frequencies in the grid cells' meteorological history. Note, however, that the robustness of such an analysis is inherently low at the local scale due to the rarity of low $NDVI$ events (Sect. 3.1). Figure 7 shows the consistency in sign of $f'^{rel}_{90d}(A)$ and $f'^{rel}_{90d}(C)$ for the 90-day periods of approximately JJA-ev (~~$n = 186$) are excluded.~~

~~Several aspects point to a contrasting meteorological storyline during event sequences as compared to single events in temperate forests. Firstly, P'_{90d} up to MAM-0m are similar for EV10 and EV11 (~~Fig. ~~??a),while $T2m'_{90d}$ is slightly increased for EV11~~ 7a,b) and MAM-3m (Fig. ~~??c). In JJA-0m, when both groups experience an event, the hot-dry anomaly is more pronounced for EV11 events . Afterwards in EV10 hot and dry anomalies gradually weaken and DJF+6m to MAM+9m~~

~~features a wet period of +0.4. The following JJA+12m exerts conditions close to climatology. In contrast, anomalies during EV11 are more pronounced and significantly different from EV10 from SON+3m to JJA+12m. While the wet period during the cold season peaks at +1.3~~7c,d), ~~P'_{90d} decreases again towards JJA+12m (Fig. ??a). $T2m'_{90}$ is by about 0.5 larger in EV11 as compared to EV10 from SON+3m until JJA+12m (Fig. ??c).Interestingly, the meteorological storylines also contrast between the one event of EV10 (in JJA-0m), and in the second event of EV11 (in JJA+12m). Despite showing a larger wet anomaly in the previous cold season, the second event of EV11 goes along with less anomalous dry conditions in JJA+12 as compared to EV10~~ respectively, for all forest grid cells that experienced at least two low $NDVI$ events in ~~JJA-0m. The same applies for the warm anomaly during JJA, and when comparing the meteorological anomalies of the second with the first event summer of EV11. These contrasts between the second event of EV11 and EV10 or the first event of EV11 in JJA are an indication of legacy effects,which are not related to the prevailing seasonal meteorology. What fosters the occurrence of another low $NDVI$ event are, therefore, either the warm anomalies more than one year back, the hot-dry anomalies in the previous JJA, or the warm-wet anomalies in the previous cold season, which were all significantly stronger for the second event of EV11 than for the first event or for EV10.~~2002–2022. The results for DJF-6m and SON-9m are shown in Appendix E.

~~Mediterranean forests show a clear sign of recovery in EV10 and fewer differences between the second event of EV11 and single events. The first clearly significant difference between the meteorological storylines of EV11~~ In the temperate biome, changes in weather system frequencies that were consistent among most or all low $NDVI$ events at one location occurred in 66–81% and in 54–64% of the considered forest grid cells in JJA-ev and ~~EV10 arises in~~ MAM-3m~~, when EV11 exerts much lower $T2m'_{90d}$~~, respectively. Most prominently, northeastern Europe showed a consistent increase of anticyclones and decrease of cyclones, respectively, in JJA-ev (Fig. 7a,b). Negative $f'^{rel}_{90d}(C)$ was consistent among all low $NDVI$ events at the southern edge of the storm track, i.e., south of the region of climatologically high $\overline{f_{90d}(C)}$ (Fig. ~~??d). Then in JJA-0m, i.e., during the first event, meteorological anomalies are not significantly different in EV11 with $(T2m'_{90d}, P'_{90d}) = (+0.6, -0.7)$ and in EV10 with $(T2m'_{90d}, P'_{90d}) = (+0.8, -0.8)$~~ 7b). In MAM-3m, however, positive $f'^{rel}_{90d}(C)$ occurred simultaneously with positive $f'^{rel}_{90d}(A)$ in Germany and parts of northwestern Europe. Positive $f'^{rel}_{90d}(A)$ in northern Europe was not only prevalent in JJA-ev, but also in MAM-3m (Fig. ~~??b,d). The meteorological storyline of EV10 after JJA-0m is characterized by more and more wet conditions, especially in MAM+9m, and only small $T2m'_{90d}$~~ (7a), in DJF-6m, and partly in SON-9m (Supplementary Fig. ~~??b,d). Contrarily, negative P'_{90d} continues over all seasons prior to the second event of EV11 and is significantly different during MAM+9m and JJA+12m. In JJA+12m, both hot and dry anomalies are similar to those in the year before~~ E1). In MAM-3m this signal further extended towards the Balkans (Fig. ~~??b,d). So it appears that event recovery is aided by positive P'_{90d} in the Mediterranean biome. The meteorological storyline of EV11 events significantly differs from that of EV10 events in terms of lower P'_{90d} after the first event.Anomalies in that time period, i. e., prior to the second event of EV11 are, to some degree, similar to the meteorological anomalies of the initial event, which does not indicate strong legacy effects.In summary, for the temperate biomes we identify signatures of potential legacy effects in both $T2m'_{90d}$~~ 7b). Southern France showed an opposite signal of increased cyclone frequency and negative $f'^{rel}_{90d}(A)$ in JJA-ev. Farther back in the meteorological history in DJF-6m and ~~P'_{90d}, while for the Mediterranean biome Fig. 7 suggests that legacy effects are less pronounced.~~ SON-9m

~~Two and a half year-evolution of (a,c) P'_{90d} and (b,d) $T2m'_{90d}$ averaged over all low $NDVI$ events in the subgroups EV10 (blue) and EV11 (brown) in (a,b) the temperate and (c,d) the Mediterranean biome. The blue shading displays the 95% confidence interval (CI) of the tested null hypothesis $H_{0,EV11}$ (see Sect. 2.4.2). EV10 exhibits an event in JJA-0m, and EV11 does so in JJA-0m and JJA+12m, as indicated by the colored horizontal bars. Vertical grey lines show the end of each season, i.e., when the seasonal average value occurs.~~

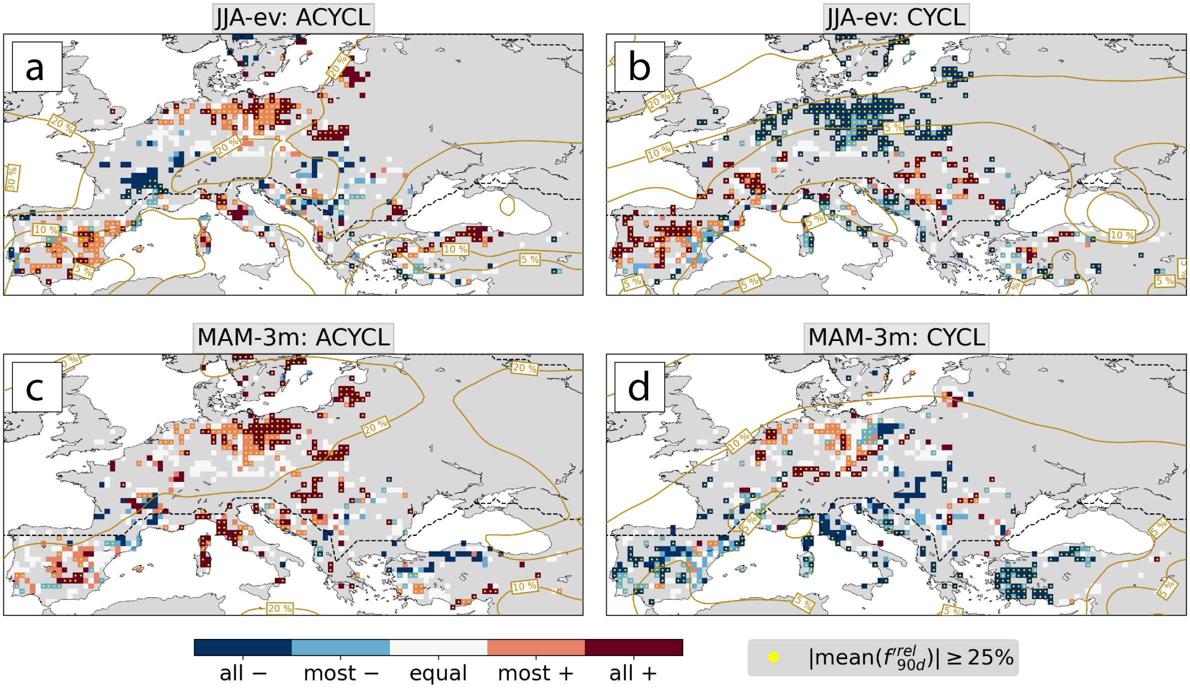

Figure 7. The consistency in sign of (a,c) $f'^{rel}_{90d}(A)$, and (b,d) $f'^{rel}_{90d}(C)$ for all forest grid cells with at least two low $NDVI$ events in 2002–2022. Maps are shown for the last day of (a,b) JJA-ev, and (c,d) MAM-3m. Stippling indicates that the absolute average over all anomalies of the same sign is at least 25%. 2D-Gaussian-smoothed (2σ) climatological weather system frequencies are shown in beige contours.

$f'^{rel}_{90d}(C)$ was negative for most or all of the low $NDVI$ events in 56–58% of the considered forest grid cells (Supplementary Fig. E2). To summarize, positive $f'^{rel}_{90d}(A)$ and negative $f'^{rel}_{90d}(C)$ were prominent features in northern Europe in the warm and cold season, respectively. Other regions, such as southern France, show interesting differences to this prominent signal.

3.4.1 ~~Bi-variate ($P'_{90d}, T2m'_{90d}$) and weather system frequencies~~

~~To conclude Sect. 3.3, we examine the bi-variate evolution of the meteorological storylines preceding low $NDVI$ events and relate it to weather system frequencies. To do so we display histograms of~~ The Mediterranean showed overall greater spatial coherence than its temperate counterpart. First of all, as Germany in MAM-3m, the ~~five ($T2m'_{90d}, P'_{90d}$) phase space compartments for the six seasons prior to low $NDVI$ events in both biomes~~ Iberian Peninsula was a region of generally increased weather system activity in JJA-ev. There was a dipole pattern of consistently positive $f'^{rel}_{90d}(C)$ in the West, and a mostly to consistently positive $f'^{rel}_{90d}(A)$ in the East (Fig. ~~??). Analogously to the analyses presented in Figs. 5 & 6 we moreover test $H_{0,EV}$ that the occurrence~~ 7a,b). This synoptic pattern fosters more frequent southerly advection. Note that the Iberian Peninsula was also a hot spot of low $NDVI$ events~~and the meteorological storyline (characterized here with the five compartments) are unrelated.Details about the spatial distribution of the seasonal phase space compartments are shown in Fig. ??. The meteorological storyline of most events is characterized by hot-dry conditions (Q2) in MAM-3m and JJA-0m (Figs. ??e,f,k,l). In both biomes, around +30% (MAM-3m) to +45% (JJA-0m) more forest regions experience Q2 than expected from the reference climatology. This mostly comes at the expense of cold-wet~~ , i.e., results there were consistent among up to six events (~~Q4) and Q0 conditions, meaning that there is a diagonal shift in the $(T2m'_{90d}, P'_{90d})$ phase space from Q4 to Q2. In the Mediterranean biome in DJF-6m, dry conditions go along with colder than usual $T2m_{90d}$, and , thus, +20% more forest regions experience cold-dry conditions instead of Q1, manifesting a diagonal shift from Q1 to Q3 (Fig. ??j). For some regions, e.g., Greece or parts of Italy, Q2 conditions only occur in DJF-6m or MAM-3m and not, as during most events, in JJA-0m (see~~ Fig. 2c). The typical signal of positive $f'^{rel}_{90d}(A)$ and negative $f'^{rel}_{90d}(C)$ occurred in the central Mediterranean in JJA-ev, and in most of Mediterranean forest grid cells in MAM-3m (Fig. ~~??d-f).~~

~~Histograms of the seasonal phase space compartments Q0–Q4 at event grid cells in (a-f) the temperate and (g-l) the Mediterranean biome, respectively, during the six seasons prior to low $NDVI$ events from MAM-15m to JJA-0m. Median and CI of the reference climatology are shown in black solid and dashed lines, respectively. Significantly anomalous frequencies are highlighted with a pink arrow indicating the direction of change.~~

~~As we have seen in earlier sections,many low $NDVI$ events in temperate forests also experience wet periods in their meteorological storyline. For 20–30% of the events, mostly occurring in central to western Europe and the Baltic,~~ 7c,d) and in DJF-6m ~~and/or SON-9m are warm-wet (~~(Supplementary Figs. ~~??c,d~~E1 & ~~??). At the biome scale, the increase of around +10% more Q1~~ E2). In these two seasons, only 5% and 6% of considered forest grid cells showed mostly or consistently positive $f'^{rel}_{90d}(C)$. Also in SON-9m~~is significantly different from the climatological reference. Note that this signal does not stem from a single event, but includes, for example, event years 2001~~, ~~2003, 2016, and 2018–2020 (Figs 2a & ??d). Further in the temperate biome, there are a few exceptional forest regions, which do not show hot-dry conditions in JJA-0m (~~cyclones were mostly less frequent than usual (Supplementary Figs. E2). Thus, Mediterranean low $NDVI$ grid cells very often experienced negative $f'^{rel}_{90d}(C)$ in the past year of the meteorological history, consistent with the results in Fig. ~~??f). This mostly relates to Q0 conditions in JJA 2020 affecting parts of western Europe, the Ukraine, and Russia. Also, a cold-wet JJA-0m occurred during the 2017 event in Russia. Lastly, in both biomes, cold-wet conditions are reduced over the entire meteorological storyline.~~ 5f. Low $NDVI$ events in the western Iberian Peninsula hot spot region, however, experienced the opposite change in cyclone frequency in JJA-ev, which might be a signal of intensified Iberian thermal lows (Santos et al., 2015).

~~While the link of weather system frequency anomalies to $T2m'_{90d}$ and P'_{90d} was rather straightforward at the biome scale (Sect. 3.3.1), the surface impact of weather systems is locally more nuanced. Details are provided in Figs. ??, ?? & ??, which show maps of the seasonal phase space compartment, the seasonal cyclone frequency anomaly $f'_{90d}(C)$, and the seasonal anticyclone frequency anomaly $f'_{90d}(A)$, respectively. Some important conclusions from these spatial considerations are:~~

– ~~In the temperate biome, the prominent (warm-)wet seasons between SON-9m and MAM-3m are accompanied by large positive $f'_{90d}(C)$ in some regions (northern Europe , the Balkans), and by weak or negative $f'_{90d}(C)$ in other regions (France, eastern Europe).~~

– ~~While hot-dry conditions in JJA-0m and JJA-12m mostly go along with positive $f'_{90d}(A)$, $f_{90d}(A)$ in western Europe is reduced by up to -10%.~~

– ~~In continental eastern Europe and the Mediterranean, cold-dry winters and hot-dry summers - both peculiarities of the meteorological storyline - are caused by more frequent anticyclones.~~

~~All in all, there is large spatiotemporal variability in the coupling of synoptic-scale weather systems and surface meteorology, consistent with findings from previous studies (e.g., Hawcroft et al., 2012; Pfahl and Wernli, 2012a; Chan et al., 2019; Röthlisberger and M~~

4 Discussion

4.1 Low $NDVI$ events

~~Events of low~~

The low $NDVI$ ~~as identified in this study typically represent summers with a~~ grid cells identified in this study typically represented summers with a heat- and/or drought-induced ~~reduction in forest performance, as shown in earlier studies (Anyamba and Tucker~~ ~~However, we also identify~~ loss of forest greenness (Anyamba and Tucker, 2012; Orth et al., 2016; Buras et al., 2020). Known drought and heat events were identified as low $NDVI$ events, e.g., the Iberian drought in 2005 (Gouveia et al., 2009), a two-year-long drought in 2007–2008 in Turkey (Varol and Ertuğrul, 2016), the 2011–2013 drought in the Balkans (Cindrić et al., 2016), the hot summer 2017 in Italy (Rita et al., 2020), and the Central European hot drought in 2018 (Schuldt et al., 2020; Senf and Seidl, 2021b). Additionally, we identify 2022 as record-breaking year of the most widespread low $NDVI$ events covering 37% of the Mediterranean and temperate forest biome each. In 2022, Europe experienced its hottest JJA on record alongside dry soils (Copernicus Climate Change Service, 2022), and the largest carbon emissions from wildfires since 2007 were recorded (Copernicus Atmos Specifically, among the countries with most low $NDVI$ grid cells were also those that faced extreme anomalies in wildfire activity; the burnt area in Romania, Germany, France, Spain, and Croatia was 11, 10, 7, 4, and 3 times larger in 2022, respectively, than the 2006–2021 average (EFFIS, 2022). First observations of early leaf senescence as in 2018 are mentioned by Kittl (2022). The regions spared by the low $NDVI$ event in 2022 - mainly Scandinavia, parts of France, and a belt from the Austrian Alps to the Baltic - were the only regions that showed a surplus in surface soil moisture compared to 1991–2020 conditions (Copernicus Climate Change Service, 2022). Our approach, therefore, not only identifies low $NDVI$ events ~~related to large-scale logging in 2009 (Senf and Seidl, 2021a),~~ due to heat and drought but also events due to positively interacting disturbances such as fire and insect outbreaks. Finally, however, there was at least one example of a drought-unrelated low $NDVI$ event, namely an ice storm ~~in~~ that hit Slovenia in February 2014 ~~(Senf and Seidl, 2021c), or cold-wet conditions in~~

~~Russia in 2017. Late frost is another potential source of~~ (Senf and Seidl, 2021c; Buras et al., 2021). Consequently, we cannot rule out that other disturbances that were not necessarily linked to heat or drought, e.g., also late frost (Bascietto et al., 2018; Vitasse et al., 2 have impacted some of the low $NDVI$ ~~, which is not related to drought (Bascietto et al., 2018; Vitasse et al., 2019).Nevertheless, large events of drought-induced decline in forest performance are well-captured by our method.Exemplary,~~ grid cells.

As our approach identifies persistent and wide-spread $NDVI$ losses, more localized and potentially more extreme reductions in forest greenness are often not captured (Appendix D), e.g., logging in France in 2009 (Senf and Seidl, 2021a), or low $NDVI$ ~~events co-occurred with reduced forest growth and carbon uptake~~ following the winter windstorm Gudrun in southern Sweden in 2005 (Buras et al., 2021). Interestingly, also the hot drought in 2003 hardly lead to low $NDVI$ grid cells in Europe. The $NDVI$ reduction in that summer was most prominent for grassland and crops but less so for forests (Buras et al., 2020). Forests are capable of resisting a temporally limited drought much better than grassland, as they can respond with reduced evapotranspiration and increased water use efficiency (Wolf et al., 2013). Note, however, that grassland is typically recovering better after long-lasting droughts than forests (Stuart-Haëntjens et al., 2018). The only forest regions that were affected by a low $NDVI$ event in 2003 ~~, and with premature leaf senescence, reduced productivity, and canopy mortality in~~ are in southern France and Italy, where strongest growth reductions in forests were observed (Ciais et al., 2005). Our results, therefore, suggest that - compared to the events since 2018 ~~(Ciais et al., 2005; Bastos et al., 2020b; Schuldt et al., 2020; Trotsiuk et al., 2020).~~ - the impact of the 2003 drought on forest greenness was generally limited and scattered in space.

~~Contrasting our~~

4.2 Meteorological histories and their inter-biome differences

The purpose of systematically analyzing meteorological histories of low $NDVI$ events ~~with forest disturbance data of Senf and Seidl (2021 more specifically canopy mortality, helps to further characterize the nature of the identified events. Large-scale windthrow, such as that during the destructive storms Lothar, Gudrun, and Kyrill, do not appear in our event set because reflectance properties of the still green understory likely dominate the~~ was to identify statistically significant meteorological precursors to these events. Hereby it should be noted that this statistical analysis alone does not allow to infer causation between the precursors and the low $NDVI$ ~~signal (McDowell et al., 2015). Nevertheless, fresh deadwood and partial tree damage from wind disturbances promote multiplication of bark beetles and , thus, may have a non-negligible effect on some of the events (Temperli et al., 2013; Jakoby et al., 2019). There is also conceptual discrepancy that arises from the fact that we only consider information at sufficiently forest-covered pixels with an area of $\sim 5\times 5\,\mathrm{km}^2$, while D is originally assessed at every $30\times 30\,\mathrm{m}^2$ pixel. Also, our aggregation method potentially ignores localized disturbances that affect less than half of the forest pixels within a $\sim 50\times 50\,\mathrm{km}^2$ grid cell, and includes~~ events, but identifies unusual co-occurrence of these precursors and the low $NDVI$ events. The causation surmised in our interpretation of these precursors below is inferred from the large body of process-focused literature we cite. We neither identify a universally valid meteorological history leading to low $NDVI$ ~~signals of only partly forest-covered pixels (Sect 2.3) . So we acknowledge that the greenness-based event set identified heremisses some forest disturbances that reduce forest performance.However, given the above-mentioned previous assessments and the~~

~~affirming event evaluation, we are confident that the event set covers large-scale reductions in forest performance in Europe in 2000–2020.~~events nor establish hitherto unknown causal links between seasonal time scale meteorology and low $NDVI$ events. Rather, the value of our approach is that we can systematically examine which aspects of the meteorological history stands out of the noise and variability that are invariably present across the large set of meteorological histories (e.g., Fig. 4) identified here.

4.3 ~~Meteorological storyline~~

The case study of low $NDVI$ grid cells in Spain in 2005 (SPA05) is one example that illustrates this value of our approach (Sect. 3.2). The meteorological history of SPA05 showed a precipitation surplus in the previous spring and summer, which was not a significant meteorological precursor to low $NDVI$ events in the Mediterranean in general (Sect. 3.3.1). A preceding surplus in precipitation in a water-limited region such as Spain could cause structural overshoot, i.e., the build-up of large crowns with high water demand, which was suggested to worsen the following drought impact (Zhang et al., 2021). Long-term irrigation experiments at dry sites revealed reduced tree growth over several years as a response to ceasing irrigation (Rigling et al., 2003; Fe Furthermore, short-term irrigation causes more pronounced responses in tree growth than long-term irrigation, while both potentially increase the sensitivity to drought in the following years indirectly via increased leaf area and tree height (Feichtinger et al., 2015 So while there is strong evidence for lagged responses to a previous precipitation surplus due to structural overshoot, our approach shows that this process does not translate to a systematic meteorological precursor at the biome scale in the Mediterranean.

~~We first mention that the complex challenge of identifying periods when ecosystems are most sensitive to meteorology has been recognized for crops too, and was successfully tackled with storyline approaches (e.g., Goulart et al., 2021). For the forest-related low~~ The most striking meteorological precursors of low $NDVI$ ~~events, statistically more prevalent dry periods in the two preceding years, and the magnitude of concurrent hot-dry conditions are common features of the meteorological storyline in the two biomes.Both signals, especially the prevalence of dry conditions~~ ~~($P'_{90d} \leq 0$)~~ ~~in the Mediterranean biome, are highly implausible when assuming no event-meteorology relationship at these lags~~grid cells were the persistence of a precipitation deficit (both biomes) and of positive temperature anomalies (temperate biome) over at least two years. Continuously dry conditions ~~are crucial and typical in the Mediterranean biome with potentially~~ reached farther back in Mediterranean than in temperate forests, which might be an important difference due to year-round growth of widespread evergreen tree species in the Mediterranean (Camarero et al., 2021). Also, ~~they~~ these conditions play an important role for forest fires, which likely ~~aggravate~~ aggravated the meteorological impact on $NDVI$ indirectly (Nagel et al., 2017; Turco et al., 2017). ~~In both biomes,~~ ~~P_{90d}~~ ~~is reduced before~~ ~~$T2m_{90d}$~~ ~~is elevated during the event year. This might follow from the fact that, especially in southern Europe, soil moisture drought in DJF and MAM increases the likelihood of a hot subsequent JJA through an enhanced soil moisture-atmosphere feedback (Seneviratne et al., 2010; Russo et al., 2019). Regardless, our results emphasize the damaging consequences of drought in the early growing season as highlighted by, e.g., Senf et al. (2020), Bigler and Vitasse (2021), and Bose et al. (2021). Despite the generally subordinate role of heat compared to drought, the~~

The identified extremely unusual accumulation of warm periods over ~~up to three years~~ around 25 months prior to events in the temperate biome points to its indirect effects on insect populations and fire, as well as to the joint amplification of drought impacts (Seidl et al., 2017; Sommerfeld et al., 2018; Seidl et al., 2020; Forzieri et al., 2021).

~~In the temperate biome, meteorological drought is interrupted by a wetter than usual period in the cold season. Warm and wet conditions in SON-9m and DJF-6m, respectively, could extend the~~ Also, because the significantly pronounced warm periods occurred in the (late) growing season of ~~the previous year. Favorable growing conditions at the margins of the growing season can exacerbate the impact on following droughts, which was shown for an early start into the growing season (Buermann et al., 2013; Bastos et al., 2020a). Furthermore, a wet-warm cold season can relate to more rain, lower snow cover, and earlier snow disappearance, which favors~~ all three preceding years, continuously increased temperatures might have worsened the impact of the event-concurrent hot drought through structural overshoot and soil moisture depletion (Bastos et al., 2020a; Zhang et al., 2021). This four-month-long hot drought in JJA-ev was of significant magnitude for both meteorological anomalies in the studied low $NDVI$ grid cells. In the Mediterranean, a large precipitation deficit preceded positive $T2m'_{90d}$ by another four months, which could follow from the fact that winter/spring drought in ~~forests (Buermann et al., 2013; Bla~~ ~~forest fire activity (Westerling, 2016). Given the prevalent dry periods in the previous year and the extended growing season, soil moisture drought likely penetrated to deeper levels (Barnard et al., 2021). Alternatively, the surplus in winter precipitation could locally foster growth in the dormant season or spring and, thus, promote larger canopy development which can aggravate the impact of the following summer drought (Bastos et al., 2020a).Both mechanisms suggest that the warm-wet interruption of the meteorological drought fosters soil moisture drought in the subsequent growing season, which is itself again characterized by low precipitation. Additionally, increased cyclone frequencies alongside warm-wet conditions possibly enhance windthrow and could indirectly foster bark beetle multiplication (Temperli et al., 2013; Biedermann et al., 2019). These results, therefore, suggest a negative legacy effect of warm-wet DJF-6m, in addition to drought legacy discussed in Sect. **??**. In the context of the drier JJA-12m and JJA-0m, these wet conditions also relate to large seasonal variability in precipitation, which has been identified as driver of tree mortality in Europe (Neumann et al., 2017)~~southern Europe increases the likelihood of a hot JJA through an enhanced soil moisture-atmosphere feedback (Seneviratne et al., 2010; Russo et al., 2019). More generally and in both biomes, the emergence of an unusually strong 90-day precipitation deficit already in spring can be particularly damaging (Senf et al., 2020; Bigler and Vitasse, 2021; Bose et al., 2021).

Apart from the accumulation of dry periods reaching far back in time in both biomes, primarily temperate forests show meteorological precursors that occurred more than one year in the past. Significantly reduced P_{90d} and increased $T2m_{90d}$ occurred during the previous JJA, which points towards drought legacy effects (Anderegg et al., 2015). This legacy might not always be reflected in $NDVI$ (Kannenberg et al., 2019), however, it can indirectly affect future forest vitality via reduced tree resilience (Bose et al., 2020). Moreover, the succession of drought in consecutive summers is particularly harmful for temperate forests, while Mediterranean forests show a decreased sensitivity to the second drought (Anderegg et al., 2020). To summarize, the systematic meteorological histories of low $NDVI$ events and differences between the two biomes can be linked to much of the current mechanistic understanding of forest vitality in the two bio-climatic regions.

4.3 ~~Weather~~ The role of weather systems~~perspective~~

Our results highlight ~~, amongst others,~~ that the timing and positioning of weather systems is crucially determining their impact on surface meteorology relevant for low $NDVI$ ~~events. The 20-month long~~ grid cells. At the biome scale, the at least 34-month-long dry period in the Mediterranean ~~biome~~ is accompanied by reduced ~~seasonal~~ 90-day cyclone frequency, ~~especially~~ most so in DJF and MAM when cyclones are climatologically most frequent (Wernli and Schwierz, 2006). Cyclones are the main contributor to cold season precipitation in these forest regions (Rüdisühli et al., 2020), and also to extreme precipitation (Pfahl and Wernli, 2012b). ~~On the other hand, more frequent anticyclones in JJA-0m likely~~ Other water-limited forest regions show a similar sensitivity to cold season precipitation, and therefore, to the precipitation-causing weather phenomenon (Williams et al., 2013). More frequent anticyclones were typical in JJA-ev and MAM-3m and relate to an upper-level subtropical ridge extending into the Mediterranean ~~, which is known to be important for heat extremes (Sousa et al., 2018; Zschenderlein et al., 2019)~~ - a known driver of heat extremes in southern Europe (Sousa et al., 2018; Zschenderlein et al Over the western Iberian Peninsula in JJA-ev, specifically, more frequent cyclones likely occurred as Iberian thermal lows that favor summer heat extremes through increased diabatic heating over the continent (Santos et al., 2015). Thus, reduced cyclone activity all along the meteorological history of Mediterranean low $NDVI$ events appears to have been the main contributor to the hot-dry meteorological precursors - with the exception of Iberian thermal lows in JJA.~~The combination of absent cyclones and more frequent anticyclones enables hot-dry conditions as during the events' meteorological storyline.~~

~~The distinct warm-wet anomaly in the temperate biome during SON-9m~~ In temperate forests, the JJA-ev and JJA-12m hot-dry conditions were both accompanied by more frequent anticyclones, especially in regions at the southern edge of the storm track. The accompanying reduction in cyclone frequency in northern Europe corresponds to ~~MAM-3m is related to more frequent cyclones. In particular, regions such as Scandinavia experience a wet anomaly with a collocated increase in cyclones corresponding to~~ a northward shift ~~in the cyclone steering jet stream(Messori et al., 2022). Some other regions in central Europe show weak or no increase in cyclone frequency, as they typically receive precipitation from fronts located outside the cyclone center (Rüdisühli et al., 2020).Hot-dry conditions during JJA are partly related to more frequent anticyclones.The~~ of the jet stream, which can lead to reduced forest greenness in these regions (Messori et al., 2022). More frequent anticyclones, on the other hand, often relate to an upper-level blocking that causes heat and precipitation suppression in central to northern Europe (Pfahl and Wernli, 2012a; Zschenderlein et al., 2019). A few regions in western Europe show an opposite signal, i.e., reduced anticyclone frequency in ~~JJA-0m in western Europe could relate~~ JJA-ev. This relates to the fact that summer precipitation ~~frequently occurs in~~ there frequently occurs within high-pressure systems (Rüdisühli et al., 2020)~~, i. e., a more northerly displaced jet stream favors reduced greenness in that region (Messori et al., 2022). An anticyclone centered over Europe often goes along with convective precipitation in its~~. In these cases, convective precipitation occurs in the moist and unstable inflow ~~over southwestern Europe (Mohr et al., 2020). Contrarily, continental to northern Europeis a region where stable European anticyclones and upper-level blocking typically cause heat waves and precipitation suppression (Pfahl and Wernli, 2012a; Zschenderlein et al~~ ~~These~~ west of the anticyclone center (Mohr et al., 2020). So while in JJA a European-centered anticyclone can favor low

$NDVI$ grid cells in northern Europe, it might be unfavorable for low $NDVI$ grid cells in western Europe. All in all, these considerations highlight the importance of weather systems and the necessity of considering their spatiotemporally varying impact on surface meteorology, also when interested in events of substantial forest impact.

4.4 ~~Drought legacy effects and event recovery~~

~~In Sect. ?? we compared single events to sequences of events and found indications of drought legacy effects in the temperate biome. Drought legacy effects are known to reduce tree-level growth (Anderegg et al., 2015), and, more broadly, resilience (Bose et al., 2020). Thus, the previous drought-induced low $NDVI$ event could be a sign of reduced tree vigor and higher susceptibility for a following drought, as detected, e.g., in 2019 (Schuldt et al., 2020; Bastos et al., 2021). Moreover, forests potentially acclimate to increased drought stress, which might also lead to reduced leaf area and productivity (Gessler et al., 2020). However, drought legacy is not always reflected in $NDVI$ (Kannenberg et al., 2019). Furthermore, it is important to remember that $P'_{90d} \leq 0$ does not necessarily indicate soil moisture drought, nor critically low precipitation sums due to normalization (Zang et al., 2020, see also Sect. 4.4). Nevertheless, our meteorological findings support that increased vulnerability to drought sequences can out-compete acclimation (Anderegg et al., 2020), and also that drought legacy effects - at least partly - reflect in $NDVI$. They further suggest that temperate forests are more sensitive to droughts in consecutive years, while Mediterranean forests show a decrease in sensitivity to the second drought in agreement with Anderegg et al. (2020).~~

~~During event recovery in both biomes, hot-dry conditions as prior to low $NDVI$ events are clearly absent. In the Mediterranean biome, seasonal precipitation is around normal in DJF and increased in MAM, which are periods of increased drought-sensitivity (Bose et al., 2021; Camarero et al., 2021). In the temperate biome, it seems that average seasonal precipitation - also in the more drought-sensitive MAM (Bose et al., 2021) - allows for forest recovery after a low $NDVI$ event. This is also supported by the fact that low $NDVI$, potentially by defoliation, can be followed by re-greening instead of mortality, depending on subsequent growing conditions (Dobbertin and Brang, 2001; Kannenberg et al., 2019; Rohner et al., 2021).~~

4.4 Caveats

The ~~main caveat~~ two main caveats of this study ~~is the short data record, which implies that we have to~~ are (i) ~~aggregate over large areas to get robust results~~the event aggregation to the comparably large scale, and (~~2) frequently perform normalization as opposed to superior statistical modelling (Sects. 2.3 & 2.4.1).~~ ii) the relatively short data record. The former implies that our analyses can neither account for species-specific drought responses (Scherrer et al., 2011; Vanoni et al., 2016), nor for the multi-dimensional nature of tree mortality (Allen et al., 2015; Etzold et al., 2016; Schuldt et al., 2020). The link between drought, drought response, and tree mortality is mediated by site, stand, and tree properties ~~(Etzold et al., 2019; Vitasse et al., 2019; Wohlgemuth et a~~ and can further be shaped by tree species diversity within a forest (Grossiord et al., 2014)~~and~~ , its micro-climate (Buras et al., 2018)~~. Also, using $NDVI$ signals at pixels with up to50% non-forest surface cover introduces some bias.Increasing this threshold, however~~, ~~does not change the identified events hot spots, and unfavorably decreases the sample size of our analyses (not shown). The large-scale approach of the study has proven useful to connect impaired forest performance with atmospheric dynamics acting at a scale much larger than the stand level~~and legacies of changing environmental conditions due to, e.g., past forest management (Thom et al., 2018). This aggregation, however, is a central element of this study as we aimed to investigate the link of synoptic atmospheric variability with variability in forest $NDVI$, which both act on very different spatial scales. The event identification is, therefore, targeted to identify only spatially coherent losses of forest $NDVI$, which are meaningful to aggregate to the larger scale. Also, the sub-sampling of the identified low $NDVI$ grid cells ascertains that our results do not highlight meteorological precursors that are unique to very few events or regions. Nevertheless, the results of this study should be confronted with more specific and local impact assessments.

~~We rely on normalization to compare $NDVI$ anomalies and the meteorological storylines~~ The main consequence of the relatively ~~scarce events~~ short data record is that the normalization of meteorological anomalies suffers from significant sampling uncertainty, which renders any comparison over space and time ~~. The normalization of $NDVI$ is less problematic as it serves a pragmatic, site-specific identification of low performance, and was additionally compared to an independent data set.~~ rather difficult. The normalized P'_{90d} and $T2m'_{90d}$ ~~, however, do~~ then not necessarily represent the actual site-level temperature and precipitation values and their interpretation requires care (Zang et al., 2020). This specifically applies when comparing the meteorological ~~storyline~~ history of the temperate with the Mediterranean biome, respectively, as the latter climatologically receives little precipitation during summer (Schultz, 2005). The ~~use of~~ normalization, however, is a way to use basic meteorological variables ~~instead of a more complex drought index is motivated by the overarching research question of this study~~that can readily be interpreted and linked to weather system dynamics, which is ~~to characterize the meteorological storyline of these events~~of great importance to the novelty of this study.

5 Conclusions

This study identified specific aspects of the meteorological ~~storyline~~ history (the three-year evolution of ~~seasonal~~ 90-day temperature, $T2m'_{90d}$, and precipitation anomalies, P'_{90d}), which ~~is characteristic for events of~~ are systematically shared characteristics of events of persistently low summer forest greenness at the 50 km scale in Europe in ~~2000–2020~~2002–2022. Forest greenness as measured by the $NDVI$ is ~~used to detect reduced forest performance -~~ also used as an early warning mechanism of forest ~~decline (Buras et al., 2021). In temperate forests,~~ dieback (Buras et al., 2021). First and foremost, in the temperate and Mediterranean biome the regions with low $NDVI$ events ~~are preluded by extraordinarily persistent warm periods, and an unusual accumulation of dry periods over two years. Most interestingly, the preceding cold season specific to such events is warm-wet, and - as we hypothesize - potentially exerts a negative legacy effect on the following summer drought.Dry and hot anomalies are both statistically significant during spring and summer leading up to the identified events~~ in 2022 exceeded the previous record summers 2018 (temperate) and 2008 (Mediterranean) by far with regard to spatial extent. In the hottest summer in Europe on record, 37% of both forest biomes were affected by persistently low $NDVI$, which is an increase of about +13% compared to the previous records. In contrast, our approach classifies the impact of the hot-dry summer 2003 on forests as very limited and, if so, scattered in space.

The approach used in this study identifies and quantifies those meteorological features that preceded many of the events in the same way and reveals considerable inter-biome differences. The persistence of dry periods was significantly increased over at least 26 and 34 months prior to low $NDVI$ events in the temperate and Mediterranean biome, respectively. ~~While the warm-wet cold season anomalies are more pronounced prior to the second event of a two-year event sequence, the following growing season is less hot and dry as compared to single events, which suggests a potential role of legacy effects from the previous~~ In contrast, the persistence of hot periods was only significantly increased (at least for 25 months preceding the events) in the temperate biome, but not the Mediterranean biome. Closer to the event summer, negative P'_{90d} and positive $T2m'_{90d}$ were significantly anomalous in magnitude. In the temperate biome, both anomalies acquired statistically significant magnitudes in spring, four months before the low $NDVI$ event. In the Mediterranean biome, ~~a quasi-uninterrupted 1.5 year-long seasonal precipitation deficit is observed~~ negative P'_{90d} arose another four months earlier, i.e., eight months prior to low summer $NDVI$~~events. These dry conditions in the Mediterranean go along with colder $T2m'_{90d}$ in winter and warmer $T2m'_{90d}$ in spring and summer~~. ~~Closer to the event summer, negative~~ Note that a single P'_{90d} ~~and positive $T2m'_{90d}$ are characteristically pronounced over the preceding nine and four months, respectively. In two-year event sequences, the seasonal precipitation deficit persists over an additional year while variations in $T2m'_{90d}$ seem to play a subordinate role~~value that was anomalous, e.g., eight months prior to the low summer $NDVI$, denotes an anomaly that refers to a 90-day period, i.e., to the eight to ten months prior to the event. Lastly, the systematic meteorological histories are able to verify whether meteorologically related processes from local observations apply to an entire biome. We discuss structural overshoot (Zhang et al., 2021), which is plausible to systematically affect low $NDVI$ events in the temperate biome through warmer or extended growing seasons. In contrast, structural overshoot due to more precipitation in the previous year is highly plausible for a case study in the water-limited Mediterranean, which, however, does not translate to the biome scale.

~~Moreover~~Finally, we provide clear evidence on the spatially varying impact of synoptic-scale weather systems ~~over time periods of up to 2.5 years on the key characteristics of the meteorological storylines~~on the important meteorological precursors. At the biome scale, ~~persistent drought is~~ the prominent dry periods are often caused by a ~~continuously~~ significantly reduced cyclone frequency ~~, and only the intermittent wet period in temperate forests relates to more frequent cyclones. In contrast,~~ in the Mediterranean biome, and by increased anticyclone frequency ~~relates to the onset and intensification of negative P'_{90d}~~in the temperate biome, respectively. This effect can, however, differ at a local scale, depending on which weather system is locally relevant for precipitation. For instance, western Europe often receives summer precipitation from convective cells in anticyclones and, thus, hot-dry conditions in the event summer go along with reduced anticyclone frequency.

The important differences between the meteorological ~~storyline~~ histories impacting temperate and Mediterranean forests as identified in this study provide a better understanding of European forests' response to multi-seasonal meteorology. ~~We could, for example, bring forward meteorological indications of drought legacy effects in the temperate forests~~Moreover, we for the first time quantify and assess the impact of the extremely hot summer 2022 and compare it with that of the preceding twenty years. Finally, the presented systematic investigations bridge the gap between forest dynamics and atmospheric dynamics, and, thereby, constitute progress in how expected forest ~~decline~~ dieback can be linked to changing meteorological and climatic conditions under global warming.

Data availability. We uploaded the low $NDVI$ events in JJA 2002–2022 as identified in this study on the ETH Research Collection (https://doi.org/20.500.11850/505559). The data sets used in this study are freely available, namely 16-daily $NDVI$ data from the NASA Application for Extracting and Exploring Analysis Ready Samples (AppEEARS; https://appeears.earthdatacloud.nasa.gov/), global forest cover area by Büttner et al. (2004, https://land.copernicus.eu/pan-european/corine-land-cover), and atmospheric fields of ERA5 from the ECMWF (https://cds.climate.copernicus.eu/cdsapp##!/dataset/reanalysis-era5-pressure-levels?tab=form). We use the updated version 1.1 of forest disturbance data (Senf and Seidl, 2021a) and aggregate the data to the ERA5 grid. Version 1.0 is available at https://doi.org/10.5281/zenodo.3925446.

Code and data availability. At https://github.com/corneliussenf/AggregateDisturbancesERA5 the code used to aggregate forest disturbance data can be accessed. All other code is available upon request.

Appendix A: ~~Bootstrapping tests~~Sensitivity to threshold parameters

~~For null hypothesis $H_{0,EV}$, we generate 10'000 synthetic event sets $EV^{r}_{J,n}$ by randomly shuffling the 21 annual chunks of $EV_{J,n}$~~ The event identification is based on three threshold parameters, namely the minimum affected ratio $AR^{min} = 80\%$, the minimum forest area $FA^{min} = 10\%$, and the minimum number of time steps in JJA with negative $NDVI'$ $n^{min}_{t,ev} = 4$ (Sect. 2.3)~~, i. e. , by assigning a random year n^r without replacement to all events in year n. The synthetic meteorological storylines (i. e. , time series of normalized meteorological anomalies $T2m'^{r}_{90d}$ and P'^{r}_{90d}) are generated by extracting ERA5 fields for $EV^{r}_{J,n}$. They are then used to identify the corresponding phase space compartment Q^{r}. As for the actual low~~. Parameter AR^{min} refers to the fraction of forest pixels that has to show persistently negative $NDVI$ ~~events, we compute~~ per $0.5° \times 0.5°$ grid cell for that grid cell to be identified as low $NDVI$ grid cell. Persistently here is defined via a lower threshold $n^{min}_{t,ev}$ for ~~each of the~~ $n_{t,ev}$, where the latter refers to the number of time steps out of a total of six in JJA that show negative $NDVI$. Lastly, FA^{min} sets a minimum forest cover per grid cell to filter out those with only very few forest $NDVI$ pixels. We vary AR^{min} and FA^{min} by $\pm 5\%$ and test different combinations thereof. We vary $n^{min}_{t,ev}$ by ± 1 only for the setup "80_10~~'000 synthetic event sets the event mean $T2m'^{r}_{90d}$,~~" used in the study ($AR^{min} = 80\%$, $FA^{min} = 10\%$) as the identification scheme depends strongly on this parameter. Table A1 shows the number of events (n_{tot}), the number of years with at least ten low $NDVI$ grid cells in 2002–2022 (n_{yr}), and also the number of events per sub-sample (n_{ev}) that result from varying the threshold parameters. Large n_{yr} is important to the sub-sampling of the low $NDVI$ grid cells, which is used to retrieve more systematic results, and would optimally be as close to the total years of 21 as possible. The n_{tot} is particularly strongly reduced when increasing AR^{min} to 85%, resulting in $n_{yr} \leq 10$. Aiming to optimize n_{yr} by using looser thresholds, however, would misconceive a typical characteristic of extreme events such as low $NDVI$ events, namely that they occur concentrated in individual years and not in others. So looser thresholds have the disadvantage of reducing the peculiarity of low $NDVI$ grid cells. This is illustrated by the ~~event mean P'^{r}_{90d},~~ $\sim 1.5\times$ increase in n_{tot} when reducing AR^{min} from 80% to 75%. While reducing $n^{min}_{t,ev}$ in the study setup (80_10) from four to three has only minor effects, n_{tot} and consequently n_{yr} and ~~the frequency $f(Q)$ among all events for every phase space compartment. The distribution spanned up by these~~ n_{ev} are drastically reduced when increasing $n^{min}_{t,ev}$ to five (Table A1). For example, in the temperate biome, only three years would contribute at least ten low $NDVI$ grid cells if $n^{min}_{t,ev} = 5$ was used. So while the number of events is not very sensitive to reductions in $n^{min}_{t,ev}$, increasing $n^{min}_{t,ev}$ would make a systematic assessment impossible.

The sensitivity of the main result to these two parameters is illustrated at the example of Fig. 5. As in the original Fig. 5, we perform a random sub-sampling of up to ten low $NDVI$ grid cells per year for each biome and compute an average meteorological history from the resulting samples (Sect. 3.3). This sub-sampling is done ten times for each biome, and Fig. A1 shows the median of these ten equivalent average meteorological histories for every of the eleven combinations of AR^{min}, FA^{min}, and $n^{min}_{t,ev}$ listed in Table A1. The sub-sampling for each combination of the two threshold parameters is of course dependent on the identified low $NDVI$ grid cells and, therefore, dependent on n_{tot} and n_{yr} (Table A1).

Table A1. Number of events (n_{tot}), number of years with at least ten low $NDVI$ grid cells (n_{yr}), and number of events per sub-sample (n_{ev}) in the temperate and Mediterranean biome for different combinations of threshold parameters. The column title indicates the setup with $n_{t,ev}^{min} = 4$ and different AR^{min} and FA^{min} combinations separated by an underscore - except for the last two columns. These denote tuning the threshold parameter $n_{t,ev}^{min}$ to three and five while $AR^{min} = 80\%$ and $FA^{min} = 10\%$.

								Sensitivity
	75_5	**75_10**	**75_15**	**80_5**	**80_10**	**80_15**	**85_5**	
$\mathbf{n_{tot}}$ **in temp.**	2294	1998	1744	1580	**1386**	1204	929	
$\mathbf{n_{yr}}$ **in temp.**	17	17	17	16	**15**	15	10 ~~'000 synthetic values gives us the reference climatologies~~ $\cancel{\overline{T2m'^{r}_{90d}}}$, $\cancel{\overline{P'^{r}_{90d}}}$,	
$\mathbf{n_{ev}}$ **in temp.**	187	185	183	173	**170**	164	138	
$\mathbf{n_{tot}}$ **in Med.**	1701	1319	1078	1287	**989**	808	861	
$\mathbf{n_{yr}}$ **in Med.**	18	16	15	16	**14**	14	12	
$\mathbf{n_{ev}}$ **in Med.**	195	187	177	177	**164**	160	155	

Figure A1 overall highlights low sensitivity of various aspects of the meteorological history on the two threshold parameters. First, the number of events per sub-sample and thus per average meteorological history n_{ev} differs for every setup of threshold parameters depending on variations in n_{tot}. Consequently, setups with more events per sample (loose thresholds) lead to smaller magnitudes of the averaged meteorological anomalies, and, hence, also a more narrow confidence interval than a setup with fewer events per sample (stricter thresholds). The comparison here, therefore, focuses mostly on aspects such as the timing and evolution of significant anomalies instead of their exact magnitude. The statistically significant anomalies highlighted in our study, e.g., negative P'_{90d} in JJA-12m and JJA-ev, and positive $T2m'_{90d}$ that emerged in MAM-3m in temperate forests, respectively, would also result from other parameter setups (Fig. A1a,c). Especially the timing when meteorological anomalies were significantly different from climatology are consistent within almost all eleven setups. Some of the highlighted anomalies persisted longer and emerged more clearly when using stricter thresholds, e.g., $AR^{min} = 85\%$ and $\cancel{f(Q)}$~~.Note that~~ $FA^{min} = 15\%$. Positive $T2m'_{90d}$ followed JJA-12m into SON-9m and also the warm period prior to JJA-ev reached farther into the past (Fig. A1c). With that setup, also the negative $f'_{90d}(C)$ in MAM-3m prior to low $NDVI$ events in the Mediterranean biome were more distinct than for the setup used. With stricter parameter setups, however, n_{ev} is unfavorably reduced as the number of years contributing the maximum of ten low $NDVI$ events (n_{yr}) is greatly reduced (Table A1). This is strongly pronounced when using the setup "5of6", for which, e.g., in the temperate biome, only three years (2018, 2019, and 2022) contribute substantially to the ~~shuffling of years is done prior to extracting the spatial fields of~~ $\cancel{T2m}$ ~~and~~ $\cancel{P}$ ~~from the ERA5 data set.This has the convenient effect that spatial correlation in these two meteorological variables is retained and synthetic meteorological storylines are, thus, constructed from a data set with exactly the same spatial correlation of~~ $\cancel{T2m}$ ~~and~~ $\cancel{P}$ ~~as the original data set . We then compare~~ average meteorological history shown in Fig. A1. Considering the numbers in Table A1 this setup can clearly not provide a meaningful evaluation of low $NDVI$ events over the study period. Apart from that setup, any larger deviation between the results from the different parameter setups typically occur within the respective confidence

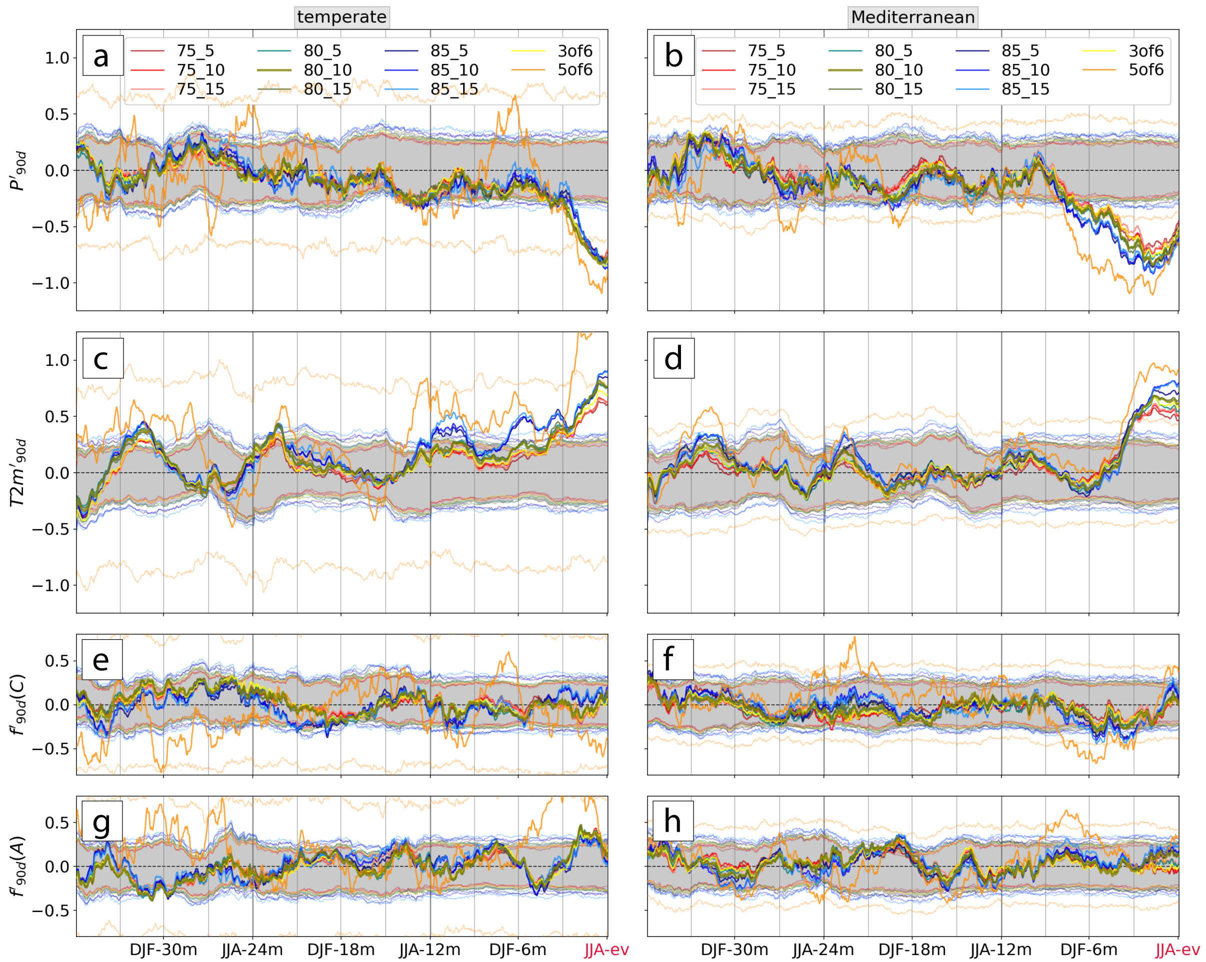

Figure A1. Same as Fig. 5 but for different combinations of AR^{min}, FA^{min}, and $n_{t,ev}^{min}$. The thicker olive line and the grey shaded 95% confidence interval (CI) correspond to the median setup shown in the study (Fig. 5). The other thick lines show the meteorological histories of the other combinations of threshold parameters, and the corresponding CI is shown with thin lines of the same color. The normalized 90-day mean (a,b) precipitation, (c,d) temperature, (e,f) cyclone frequency, and (g,h) anticyclone frequency anomalies $f'_{90d}(C)$ and $f'_{90d}(A)$, respectively, are shown as line plots. The legend indicates the combination of threshold parameters used as in Table A1.

intervals - e.g., $f'_{90d}(A)$ in JJA-ev - and are, hence, not highlighted in the analysis and interpretation of Fig. 5. To summarize, the sensitivity analysis supports the chosen setup with $AR^{min} = 80\%$, $FA^{min} = 10\%$, and $n_{t,ev}^{min} = 4$, and generally demonstrates low sensitivity of the main results to reasonable variations in the three parameters.

Appendix B: Bootstrapping tests

In the bootstrapping test we want to test the null hypothesis $H_{0,EV}$ that a given aspect X of the meteorological history at $t_{ev} - \Delta t$ is unrelated to the occurrence of low $NDVI$ events at t_{ev}. For X we use the meteorological fields of $T2m'_{90d}$, P'_{90d}, $f'_{90d}(C)$, $f'_{90d}(A)$, as well as the fraction of Δt where $T2m'_{90d} > 0$ and ~~$f(Q)$ of low~~ $P'_{90d} < 0$, respectively, covering 1999–2022 and the study domain (Fig. 1a). The fields are used here for the period 1999—2022, in order to compute three-year meteorological histories for all low $NDVI$ ~~events to the 10~~events in 2002-–2022. Figure B1 illustrates the procedure of retrieving event mean meteorological histories as well as the way the bootstrapping is constructed.

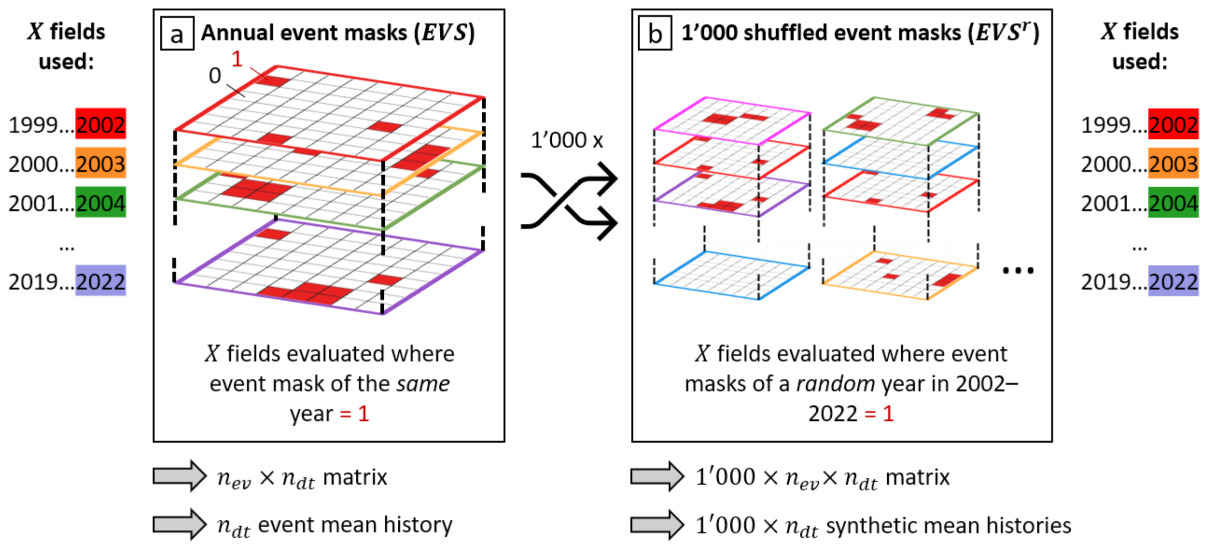

Figure B1. Schematic of the construction of the event-mean meteorological histories (a) of event set EVS, and of (b) their synthetic analogues EVS^r used for the bootstrapping test. The rows on the side show the order in which fields of X are used to extract the time series for EVS and each EVS^r. The annual binary event masks of EVS in (a) are colored according to the year of occurrence. The shuffled EVS^r have a different order of these masks, however, use the X fields in the same order as EVS.

First, the sub-sampling of all low $NDVI$ grid cells results in an event set EVS of low $NDVI$ grid cells that can be represented as three-dimensional binary $21 \times n_{lat} \times n_{lon}$ event mask, which is equal to 1 at every low $NDVI$ grid cell (Fig. B1a). Further, for every X we retrieve an $n_{ev} \times n_{dt}$ matrix - i.e., one with a time series with $n_{dt} = 3 \times 365$ daily time steps for every of the n_{ev} selected low $NDVI$ grid cells - by extracting the fields of X where EVS equals 1. The average time series of X for one sample results from taking the mean along the first dimension of this matrix, as shown in Fig. 5. For the bootstrapping test, we generate 1'000 ~~$T2m'^{r}_{90d}$~~synthetic event sets (EVS^r) by randomly shuffling the 21 annual masks of EVS 1'000 times (Fig. B1b). This shuffling process is best visualized by shuffling a deck of cards, whereby each card corresponds to a the binary $n_{lat} \times n_{lon}$ event mask of a specific year. Specifically, when constructing the random event set with number

r we assign a randomly selected year y_i^r to all low $NDVI$ grid cells occurring in year y_i and then repeat the process for all remaining years. Hereby, the random years are chosen such that each year occurs once in every EVS^r. Consequently, each reference event set contains the same number of low $NDVI$ grid cells as EVS but in a different year-location combination. Afterwards, the synthetic meteorological histories are generated by first retrieving X^r from extracting X fields for EVS^r, i.e., using the shuffled deck of annual binary event masks. Then, the resulting $1'000 \times n_{ev} \times n_{dt}$ matrix is averaged along its second dimension to retrieve a set of 1'000 synthetic event-mean time series for every X^r. We, ~~P'^r_{90d}, and Q^r, respectively. Values~~ thereby, create 1'000 meteorological histories that are equally plausible in the climatological reference period without the prerequisite of a following low $NDVI$.

We then compare event-mean time series of X of low $NDVI$ grid cells to the 1'000 synthetic event-mean time series of X^r. Values of X outside the range of ~~$T2m'^r_{90d}$, P'^r_{90d}, and Q^r~~ X^r receive a p-value of 0 (Röthlisberger et al., 2016). The remaining p-values are estimated from the percentiles of the ~~synthetic data set~~ $1'000 \times n_{dt}$ synthetic matrix along its first dimension. At the significance level of ~~$\alpha = 5\%$~~ $\alpha = 5\%$, $H_{0,EV}$ is rejected at time lags Δt if the event value of X is outside the 95% confidence interval~~of the reference climatologies.~~, i.e., outside the $2.5^{\text{th}} - 97.5^{\text{th}}$ percentile range, of the 1'000 reference values of X^r. Note that the shuffling of years is done prior to extracting the spatial fields of X from the ERA5 data set. This has – in contrast to a random sampling of all forest grid cells – the convenient effect that spatial correlation in these meteorological variables is retained. Thus, synthetic meteorological histories of X^r are constructed from a data set with exactly the same spatial correlation as the original data sets of X.

~~For null hypothesis $H_{0,EV11}$, we generate 10'000 synthetic event sets $EV10^r_{J,n}$ by drawing samples with n_{EV11} =73 (19) from the original event set $EV10_{J,n}$ with n_{EV10} =971 (282) in the temperate (Mediterranean) biome. $T2m$ and P data is again extracted 10'000 times for $EV10^r_{J,n}$ yielding a reference of EV10-type meteorological storylines. The $H_{0,EV11}$ (that there is no difference in $T2m'_{90d}$ / P'_{90d} between EV10 and EV11) is rejected for all time lags Δt at which the events $T2m'_{90d}$ / P'_{90d} lies outside the $2.5^{th} - 97.5^{th}$ percentile of the 10'000 reference values.~~

Appendix C: Low NDVI events and forest disturbance

Appendix D: ~~Low $NDVI$ events and forest disturbances~~

We provide a brief and qualitative comparison of our set of low $NDVI$ grid cells with the independent disturbance data set of Senf and Seidl (2021a). The comparison is useful to put the identified low $NDVI$ events into perspective regarding existing knowledge on forest disturbances.

~~Disturbance anomaly D' at all overlapping forest grid cells in selected years (shading). The stippling indicates low $NDVI$ events during JJA. Tracks of cyclones mentioned in the text, which occurred in the previous autumn or winter, are shown in black, with 3-hourly core pressure in hPain colored dots. The location and extent of the cyclone at time of lowest core pressure is shown in cyan.~~

C1 Forest disturbance data set

~~Figure **??** presents forest disturbance anomalies D' (Sect. **??**) for selected years together with low $NDVI$ events (Sect. 2.3). In years of widespread low $NDVI$ events, namely 2018, 2020, 2019, and 2003, the event coverage largely agrees with regions of positive D' (Fig. **??**b, f-h). As noted~~ We use the forest disturbance data set by Senf and Seidl (2021a) with an original resolution of 30 m. It is based on a time-series segmentation approach called LandTrendr (Kennedy et al., 2010) and identifies tree canopy mortality in 1986–2020. The approach uses two spectral bands (shortwave infrared I and II) and two spectral indices (tasselled cap wetness and normalized burn ratio) from Tier 1 Landsat 4, 5, 7, and 8 images in Jun–Sep. For more details see Senf and Seidl (2021a). From this data set we use the annual disturbance area $D_{J,n}$, which is aggregated for every $0.5° \times 0.5°$ forest grid cell. We only use years and grid cells that overlap with our study period and forest grid cells as identified in Sect. ~~**??**, an important source of discrepancy between the two data sets is windthrow. For example, storm Lothar in December 1999 caused catastrophic damage reflecting in extremely high D' over parts of France, Germany, and Switzerland in the following year (Fig. **??**a; Usbeck et al., 2010). Other examples were the devastating storms Gudrun affecting southern Sweden in January 2005, Kyrill in Central Europe in January 2007, and Vaia in northern Italy in October 2018 (Valinger and Fridman, 2011; Senf and Seidl, 2021c). The latter manifests in low D'~~ 2.1. Our event data set overlaps with the disturbance data set in the time period of 2002–2020 at 91% of forest grid cells as D does not cover Turkey. Consequently, 66% and 51% of all low $NDVI$ grid cells in the temperate and Mediterranean biome are compared to the disturbance data set. More specifically, we use two measures of D: the disturbance anomaly D', and the rank of D among the 19 annual values $DR_{J,n}$ in 2002–2020:

$$D'_{J,n} = \frac{D_{J,n} - \overline{D_J}}{\overline{D_J}} \quad \text{(C1)}$$

$$DR_{J,n} = rank(D_{J,n}) \quad \text{(C2)}$$

at forest grid cell J in year n, with $\overline{D_J}$ denoting the climatological mean disturbance area in 2002–2020. When referring to low $NDVI$ grid cells in the following ~~year 2019 (Fig. **??**g). Similar to our data set, the acquisition period of~~ , we thereby only address those that spatially overlap with D ~~was in summer and increased canopy mortality following autumn or winter storms is reflected in the subsequent year (Senf and Seidl, 2021a).The tracks of the four cyclones in their month of occurrence are, thus, shown for the following summer (~~data in 2002–2020.

C2 Qualitative comparison

In 70% of all low $NDVI$ grid cells the disturbance area D is larger than on average in 2002–2020 - more often in the temperate (76%) than in the Mediterranean biome (59%; Fig. ~~??~~C1a,c~~,d,g). Regions of large~~). The median disturbed area increases by +27% and +16% during low $NDVI$ events in the temperate and Mediterranean biome, respectively. Furthermore, non-events typically go along with negative D' ~~are typically located at the southern or eastern flank of the cyclones,where typically their fronts propagate, at around the time when they reach their lowest core pressure. Lastly, human influence is another source of disagreement between D and~~ in the temperate (61% of non-events) and the Mediterranean biome (66%). Figure C1b,d additionally shows the disturbance area rank, DR, from 1 (smallest D in 2002–2020) to 19 (largest D). With 1–6 events per affected forest grid cell (Fig. 2c) a low $NDVI$ grid cell would go along with DR 14–19 if the event years were equal to the years of largest disturbed area. The majority of low $NDVI$ ~~, as, for example, salvage logging following wind disturbances in the Gascony in southwestern France in 2009 (Fig. ??e; Senf and Seidl, 2021a).~~ grid cells indeed cover ranks 16–19 and 15–19 in the temperate and Mediterranean biome, respectively. We conclude that low $NDVI$ grid cells tend to go along with more forest disturbances, i.e., enhanced canopy mortality, and rank among the largest forest disturbances at forest grid cells.

Appendix D: ~~Seasonal phase space compartment~~

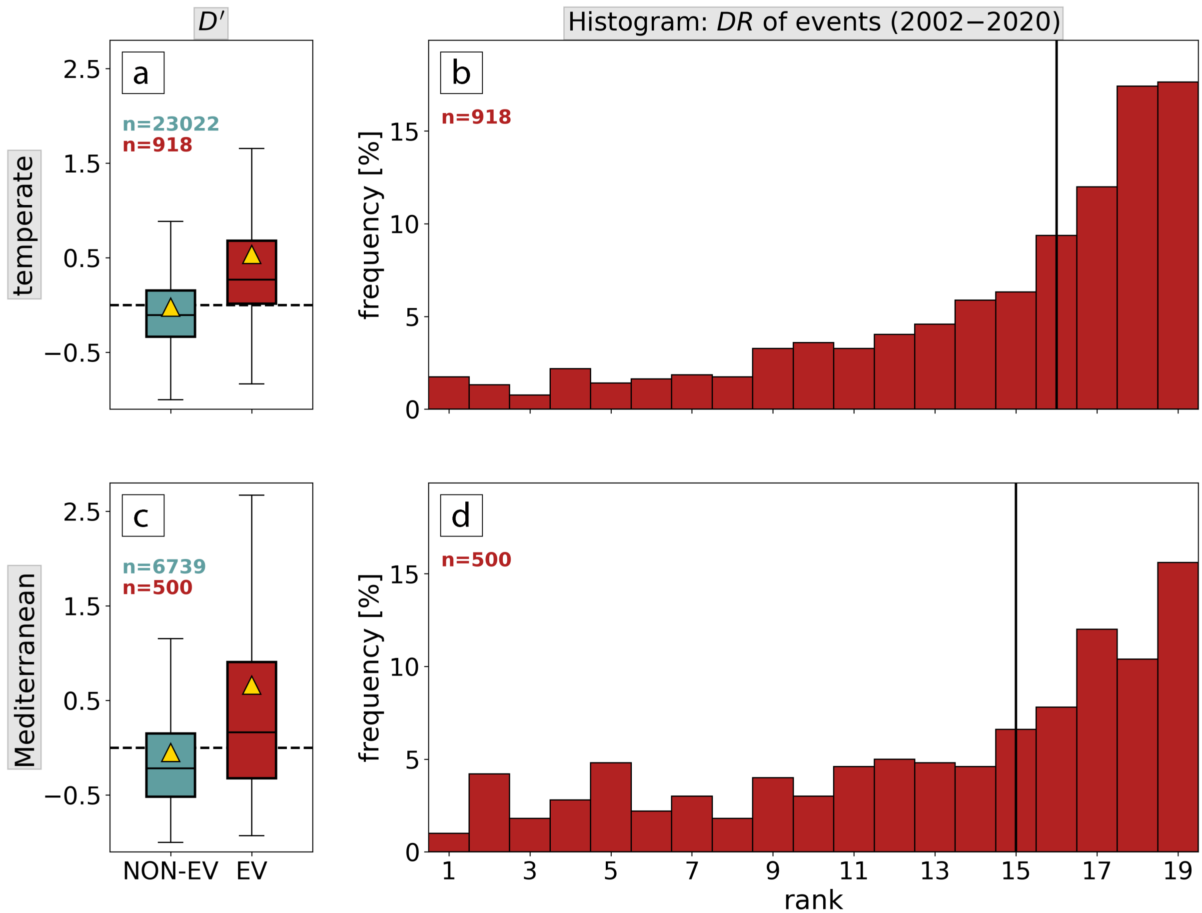

Figure C1. ~~As Fig. 2a~~ Event comparison for (a,b) the ~~seasonal ($T2m'_{90d}, P'_{90d}$) phase space compartment~~ temperate and (c,d) the Mediterranean biome in the ~~six seasons preceding~~ period 2002–2020. (a,c) box plots of the disturbance anomaly D' of low $NDVI$ ~~events~~grid cells (red) and non-event grid cells (turquoise). ~~See Fig~~The distribution mean is shown by a yellow triangle, outliers are omitted. ~~?? for biome-wide averages and statistical evaluation~~(b,d) histograms of ranks 1–19 of disturbance area DR of low $NDVI$ grid cells in 2002–2020. The median is shown by the vertical line.

Appendix D: ~~Seasonal cyclone frequency anomalies~~Maps of low $NDVI$ grid cells

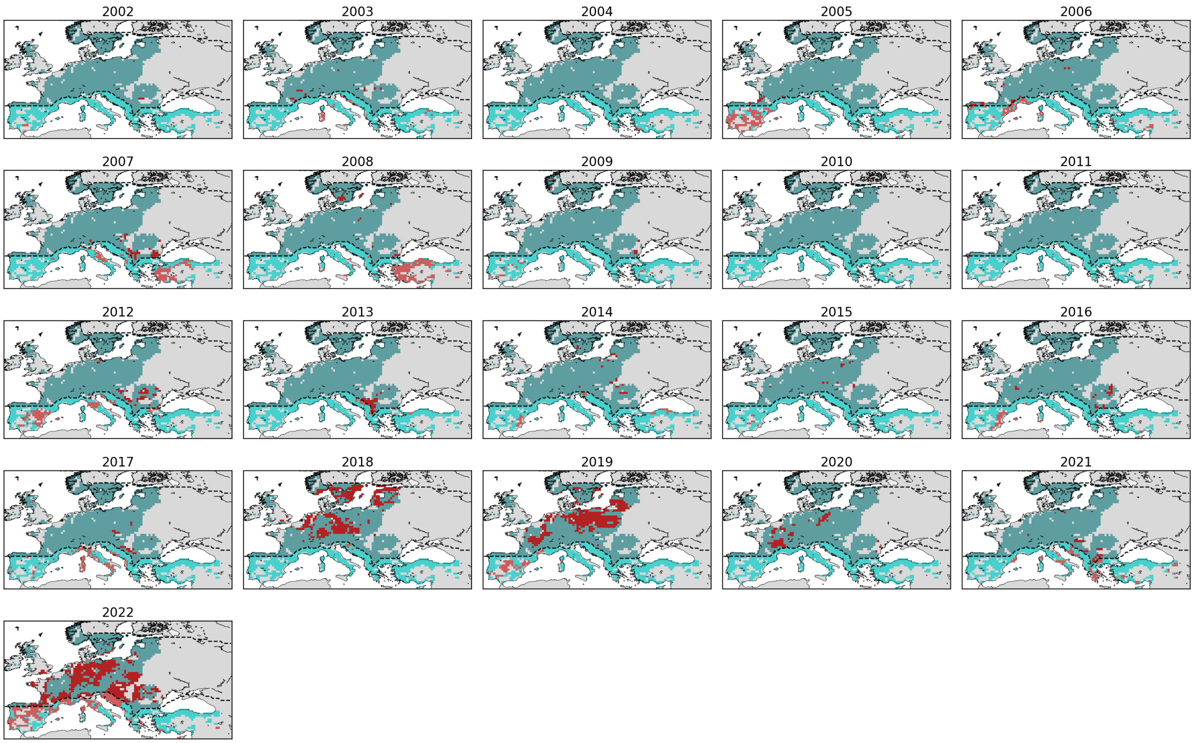

Figure D1. ~~As Fig. 2a for seasonal cyclone frequency anomalies $f'_{90d}(C)$~~ Low $NDVI$ grid cells in 2002–2022 (red) in forest grid cells of the ~~ten seasons preceding low $NDVI$ events~~temperate (turquoise) and Mediterranean biome (cyan). ~~For biome-wide averages see Fig~~The dashed lines delineate the two biomes.~~5.~~

Appendix E: ~~Seasonal anticyclone frequency~~ Weather system anomalies

The following Figures E1 & E2 show the spatial pattern of weather system anomalies. For all forest grid cells with at least two low $NDVI$ events in 2002–2022, we show how many of these events were linked to positive or negative anomalies in f'^{rel}_{90d}. Additionally, we calculate the average anomaly over all events that had the same sign of the anomaly and highlight those with mean changes of at least 25%. For each season of the past year, from JJA-ev backward to SON-9m, we use the value of f'^{rel}_{90d} at the last day of the season, which is approximately equal to the seasonal average over the three preceding months.

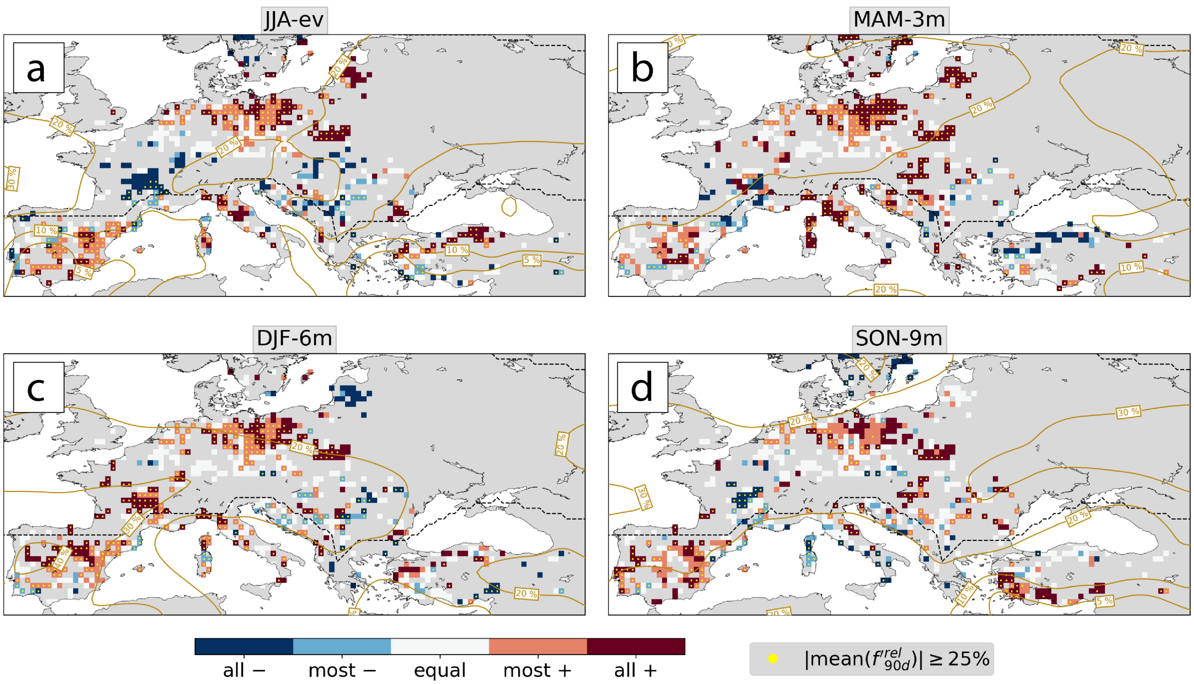

Figure E1. ~~As~~ The same as Fig. ~~??~~ 7 but for ~~seasonal~~ the relative anticyclone frequency ~~anomalies $f'_{90d}(A)$~~anomaly $f'^{rel}_{90d}(A)$ in (a) JJA-ev, (b) MAM-3m, (c) DJF-6m, and (d) SON-9m.~~For biome-wide averages see Fig. 5.~~

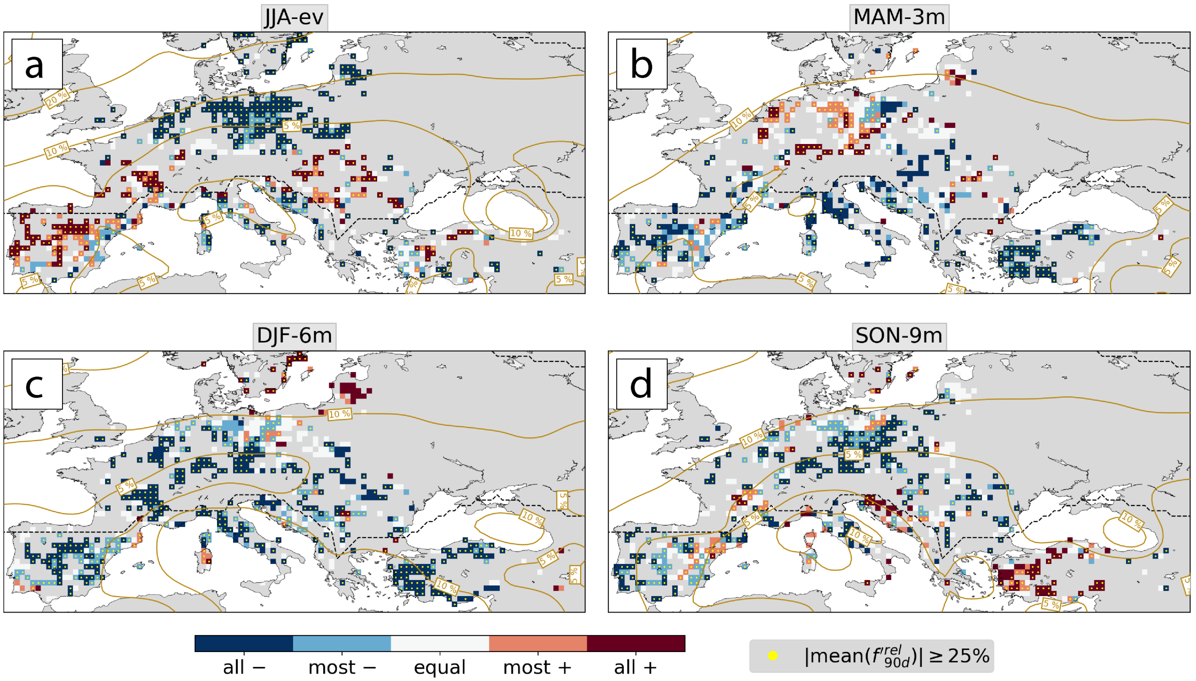

Figure E2. The same as Fig. 7 but for the relative cyclone frequency anomaly $f'^{rel}_{90d}(C)$ in (a) JJA-ev, (b) MAM-3m, (c) DJF-6m, (d) SON-9m.

Author contributions. MH performed most of the analyses and wrote a first version of the manuscript in close exchange with MR and HW. CS contributed data to the study. All authors contributed to the design of the study, the interpretation of the results, and the writing.

Competing interests. The authors declare that they have no conflict of interest.

References

Acker, J. G. and Leptoukh, G.: Online Analysis Enhances Use of NASA Earth Science Data, Eos, Transactions American Geophysical Union, 88, 14, https://doi.org/10.1029/2007EO020003, 2007.

Ali, S. M., Martius, O., and Röthlisberger, M.: Recurrent Rossby Wave Packets Modulate the Persistence of Dry and Wet Spells Across the Globe, Geophysical Research Letters, 48, https://doi.org/10.1029/2020GL091452, 2021.

Allen, C. D., Macalady, A. K., Chenchouni, H., Bachelet, D., McDowell, N., Vennetier, M., Kitzberger, T., Rigling, A., Breshears, D. D., Hogg, E. T., Gonzalez, P., Fensham, R., Zhang, Z., Castro, J., Demidova, N., Lim, J.-H., Allard, G., Running, S. W., Semerci, A., and Cobb, N.: A global overview of drought and heat-induced tree mortality reveals emerging climate change risks for forests, Forest Ecology and Management, 259, 660–684, https://doi.org/10.1016/j.foreco.2009.09.001, 2010.

Allen, C. D., Breshears, D. D., and McDowell, N. G.: On underestimation of global vulnerability to tree mortality and forest die-off from hotter drought in the Anthropocene, Ecosphere, 6, 129, https://doi.org/10.1890/ES15-00203.1, 2015.

Anderegg, W. R. L., Schwalm, C., Biondi, F., Camarero, J. J., Koch, G., Litvak, M., Ogle, K., Shaw, J. D., Shevliakova, E., Williams, A. P., Wolf, A., Ziaco, E., and Pacala, S.: Pervasive drought legacies in forest ecosystems and their implications for carbon cycle models, Science, 349, 528–532, https://doi.org/10.1126/science.aab1833, 2015.

Anderegg, W. R. L., Trugman, A. T., Badgley, G., Konings, A. G., and Shaw, J.: Divergent forest sensitivity to repeated extreme droughts, Nature Climate Change, 10, 1091–1095, https://doi.org/10.1038/s41558-020-00919-1, 2020.

Anyamba, A. and Tucker, C. J.: Historical perspective of AVHRR NDVI and vegetation drought monitoring, in: Remote Sensing of Drought: Innovative Monitoring Approaches, edited by Wardlow, B. D., Anderson, M. C., and Verdin, J. P., pp. 23–50, CRC Press/Taylor & Francis, Boca Raton, Florida, USA, 2012.

Barnard, D., Germino, M., Bradford, J., O'Connor, R., Andrews, C., and Shriver, R.: Are drought indices and climate data good indicators of ecologically relevant soil moisture dynamics in drylands?, Ecological Indicators, 133, 108 379, https://doi.org/10.1016/j.ecolind.2021.108379, 2021.

Bascietto, M., Bajocco, S., Mazzenga, F., and Matteucci, G.: Assessing spring frost effects on beech forests in Central Apennines from remotely-sensed data, Agricultural and Forest Meteorology, 248, 240–250, https://doi.org/10.1016/j.agrformet.2017.10.007, 2018.

Bastos, A., Ciais, P., Park, T., Zscheischler, J., Yue, C., Barichivich, J., Myneni, R. B., Peng, S., Piao, S., and Zhu, Z.: Was the extreme Northern Hemisphere greening in 2015 predictable?, Environmental Research Letters, 12, 044 016, https://doi.org/10.1088/1748-9326/aa67b5, 2017.

Bastos, A., Ciais, P., Friedlingstein, P., Sitch, S., Pongratz, J., Fan, L., Wigneron, J. P., Weber, U., Reichstein, M., Fu, Z., Anthoni, P., Arneth, A., Haverd, V., Jain, A. K., Joetzjer, E., Knauer, J., Lienert, S., Loughran, T., McGuire, P. C., Tian, H., Viovy, N., and Zaehle, S.: Direct and seasonal legacy effects of the 2018 heat wave and drought on European ecosystem productivity, Science Advances, 6, eaba2724, https://doi.org/10.1126/sciadv.aba2724, 2020a.

Bastos, A., Fu, Z., Ciais, P., Friedlingstein, P., Sitch, S., Pongratz, J., Weber, U., Reichstein, M., Anthoni, P., Arneth, A., Haverd, V., Jain, A., Joetzjer, E., Knauer, J., Lienert, S., Loughran, T., McGuire, P. C., Obermeier, W., Padrón, R. S., Shi, H., Tian, H., Viovy, N., and Zaehle, S.: Impacts of extreme summers on European ecosystems: a comparative analysis of 2003, 2010 and 2018, Philosophical Transactions of the Royal Society B: Biological Sciences, 375, 20190 507, https://doi.org/10.1098/rstb.2019.0507, 2020b.

Bastos, A., Orth, R., Reichstein, M., Ciais, P., Viovy, N., Zaehle, S., Anthoni, P., Arneth, A., Gentine, P., Joetzjer, E., Lienert, S., Loughran, T., McGuire, P. C., O, S., Pongratz, J., and Sitch, S.: Vulnerability of European ecosystems to two compound dry and hot summers in 2018 and 2019, Earth System Dynamics, 12, 1015–1035, https://doi.org/10.5194/esd-12-1015-2021, 2021.

Biedermann, P. H., Müller, J., Grégoire, J.-C., Gruppe, A., Hagge, J., Hammerbacher, A., Hofstetter, R. W., Kandasamy, D., Kolarik, M., Kostovcik, M., Krokene, P., Sallé, A., Six, D. L., Turrini, T., Vanderpool, D., Wingfield, M. J., and Bässler, C.: Bark Beetle Population Dynamics in the Anthropocene: Challenges and Solutions, Trends in Ecology & Evolution, 34, 914–924, https://doi.org/10.1016/j.tree.2019.06.002, 2019.

Bigler, C. and Vitasse, Y.: Premature leaf discoloration of European deciduous trees is caused by drought and heat in late spring and cold spells in early fall, Agricultural and Forest Meteorology, 307, 108 492, https://doi.org/10.1016/j.agrformet.2021.108492, 2021.

Blankinship, J. C., Meadows, M. W., Lucas, R. G., and Hart, S. C.: Snowmelt timing alters shallow but not deep soil moisture in the Sierra Nevada, Water Resources Research, 50, 1448–1456, https://doi.org/10.1002/2013WR014541, 2014.

Bose, A. K., Gessler, A., Bolte, A., Bottero, A., Buras, A., Cailleret, M., Camarero, J. J., Haeni, M., Hereş, A., Hevia, A., Lévesque, M., Linares, J. C., Martinez-Vilalta, J., Matías, L., Menzel, A., Sánchez-Salguero, R., Saurer, M., Vennetier, M., Ziche, D., and Rigling, A.: Growth and resilience responses of Scots pine to extreme droughts across Europe depend on predrought growth conditions, Global Change Biology, 26, 4521–4537, https://doi.org/10.1111/gcb.15153, 2020.

Bose, A. K., Scherrer, D., Camarero, J. J., Ziche, D., Babst, F., Bigler, C., Bolte, A., Dorado-Liñán, I., Etzold, S., Fonti, P., Forrester, D. I., Gavinet, J., Gazol, A., de Andrés, E. G., Karger, D. N., Lebourgeois, F., Lévesque, M., Martínez-Sancho, E., Menzel, A., Neuwirth, B., Nicolas, M., Sanders, T. G., Scharnweber, T., Schröder, J., Zweifel, R., Gessler, A., and Rigling, A.: Climate sensitivity and drought seasonality determine post-drought growth recovery of Quercus petraea and Quercus robur in Europe, Science of The Total Environment, 784, 147 222, https://doi.org/10.1016/j.scitotenv.2021.147222, 2021.

Brodribb, T. J., Powers, J., Cochard, H., and Choat, B.: Hanging by a thread? Forests and drought, Science, 368, 261–266, https://doi.org/10.1126/science.aat7631, 2020.

Buermann, W., Bikash, P. R., Jung, M., Burn, D. H., and Reichstein, M.: Earlier springs decrease peak summer productivity in North American boreal forests, Environmental Research Letters, 8, 024 027, https://doi.org/10.1088/1748-9326/8/2/024027, 2013.

Buras, A., Schunk, C., Zeiträg, C., Herrmann, C., Kaiser, L., Lemme, H., Straub, C., Taeger, S., Gößwein, S., Klemmt, H.-J., and Menzel, A.: Are Scots pine forest edges particularly prone to drought-induced mortality?, Environmental Research Letters, 13, 025 001, https://doi.org/10.1088/1748-9326/aaa0b4, 2018.

Buras, A., Rammig, A., and Zang, C. S.: Quantifying impacts of the 2018 drought on European ecosystems in comparison to 2003, Biogeosciences, 17, 1655–1672, https://doi.org/10.5194/bg-17-1655-2020, 2020.

Buras, A., Rammig, A., and Zang, C. S.: The European Forest Condition Monitor: Using Remotely Sensed Forest Greenness to Identify Hot Spots of Forest Decline, Frontiers in Plant Science, 12, https://doi.org/10.3389/fpls.2021.689220, 2021.

Büttner, G., Feranec, J., Jaffrain, G., Mari, L., Maucha, G., and Soukup, T.: The CORINE Land Cover 2000 project, http://eproceedings.uni-oldenburg.de/website/vol03%5F3/03%5F3%5Fbuttner2%2Ehtml, accessed at 26-September-2022, 2004.

Camarero, J. J., Álvaro Rubio-Cuadrado, and Gazol, A.: Climate windows of intra-annual growth and post-drought recovery in Mediterranean trees, Agricultural and Forest Meteorology, 308-309, 108 606, https://doi.org/10.1016/j.agrformet.2021.108606, 2021.

Chan, P., Hassanzadeh, P., and Kuang, Z.: Evaluating Indices of Blocking Anticyclones in Terms of Their Linear Relations With Surface Hot Extremes, Geophysical Research Letters, 46, 4904–4912, https://doi.org/10.1029/2019GL083307, 2019.

Ciais, P., Reichstein, M., Viovy, N., Granier, A., Ogée, J., Allard, V., Aubinet, M., Buchmann, N., Bernhofer, C., Carrara, A., Chevallier, F., Noblet, N. D., Friend, A. D., Friedlingstein, P., Grünwald, T., Heinesch, B., Keronen, P., Knohl, A., Krinner, G., Loustau, D., Manca, G., Matteucci, G., Miglietta, F., Ourcival, J. M., Papale, D., Pilegaard, K., Rambal, S., Seufert, G., Soussana, J. F., Sanz, M. J., Schulze, E. D., Vesala, T., and Valentini, R.: Europe-wide reduction in primary productivity caused by the heat and drought in 2003, Nature, 437, 529–533, https://doi.org/10.1038/nature03972, 2005.

Cindrić, K., Prtenjak, M. T., Herceg-Bulić, I., Mihajlović, D., and Pasarić, Z.: Analysis of the extraordinary 2011/2012 drought in Croatia, Theoretical and Applied Climatology, 123, 503–522, https://doi.org/10.1007/s00704-014-1368-8, 2016.

Copernicus Atmosphere Monitoring Service: Europe's summer wildfire emissions highest in 15 years, https://atmosphere.copernicus.eu/europes-summer-wildfire-emissions-highest-15-years, accessed at 21-October-2022, 2022.

Copernicus Climate Change Service: Copernicus: Summer 2022 Europe's hottest on record, https://climate.copernicus.eu/copernicus-summer-2022-europes-hottest-record, accessed at 10-October-2022, 2022.

Didan, K.: MOD13Q1 MODIS/Terra Vegetation Indices 16-Day L3 Global 250m SIN Grid V006, https://doi.org/10.5067/MODIS/MOD13Q1.006, accessed at 26-September-2022, 2015.

Dobbertin, M. and Brang, P.: Crown defoliation improves tree mortality models, Forest Ecology and Management, 141, 271–284, https://doi.org/10.1016/S0378-1127(00)00335-2, 2001.

EFFIS: EFFIS Estimates for European Union, https://effis.jrc.ec.europa.eu/apps/effis.statistics/estimates, accessed at 21-October-2022, 2022.

Etzold, S., Wunder, J., Braun, S., Rohner, B., Bigler, C., Abegg, M., and Rigling, A.: Mortalität von Waldbäumen: Ursache und Trends, in: Wald im Klimawandel. Grundlagen für Adaptationsstrategien, edited by Pluess, A. R., Augustin, S., and Brang, P., pp. 177–197, Haupt Verlag, Bern, Stuttgart, Wien, 2016.

Etzold, S., Ziemińska, K., Rohner, B., Bottero, A., Bose, A. K., Ruehr, N. K., Zingg, A., and Rigling, A.: One century of forest monitoring data in Switzerland reveals species- and site-specific trends of climate-induced tree mortality, Frontiers in Plant Science, 10, 307, https://doi.org/10.3389/fpls.2019.00307, 2019.

Feichtinger, L. M., Eilmann, B., Buchmann, N., and Rigling, A.: Growth adjustments of conifers to drought and to century-long irrigation, Forest Ecology and Management, 334, 96–105, https://doi.org/10.1016/j.foreco.2014.08.008, 2014.

Feichtinger, L. M., Eilmann, B., Buchmann, N., and Rigling, A.: Trait-specific responses of Scots pine to irrigation on a short vs long time scale, Tree Physiology, 35, 160–171, https://doi.org/10.1093/treephys/tpu114, 2015.

Fischer, E. M., Seneviratne, S. I., Vidale, P. L., Lüthi, D., and Schär, C.: Soil Moisture–Atmosphere Interactions during the 2003 European Summer Heat Wave, Journal of Climate, 20, 5081–5099, https://doi.org/10.1175/JCLI4288.1, 2007.

Forzieri, G., Girardello, M., Ceccherini, G., Spinoni, J., Feyen, L., Hartmann, H., Beck, P. S. A., Camps-Valls, G., Chirici, G., Mauri, A., and Cescatti, A.: Emergent vulnerability to climate-driven disturbances in European forests, Nature Communications, 12, 1081, https://doi.org/10.1038/s41467-021-21399-7, 2021.

Frei, E. R., Gossner, M. M., Vitasse, Y., Queloz, V., Dubach, V., Gessler, A., Ginzler, C., Hagedorn, F., Meusburger, K., Moor, M., Vives, E. S., Rigling, A., Uitentuis, I., von Arx, G., and Wohlgemuth, T.: European beech dieback after premature leaf senescence during the 2018 drought in northern Switzerland, Plant Biology, https://doi.org/10.1111/plb.13467, 2022.

Gessler, A., Bottero, A., Marshall, J., and Arend, M.: The way back: recovery of trees from drought and its implication for acclimation, New Phytologist, 228, 1704–1709, https://doi.org/10.1111/nph.16703, 2020.

Goulart, H. M. D., van der Wiel, K., Folberth, C., Balkovic, J., and van den Hurk, B.: Storylines of weather-induced crop failure events under climate change, Earth System Dynamics, 12, 1503–1527, https://doi.org/10.5194/esd-12-1503-2021, 2021.

Gouveia, C., Trigo, R. M., and DaCamara, C. C.: Drought and vegetation stress monitoring in Portugal using satellite data, Natural Hazards and Earth System Sciences, 9, 185–195, https://doi.org/10.5194/nhess-9-185-2009, 2009.

Grossiord, C., Granier, A., Ratcliffe, S., Bouriaud, O., Bruelheide, H., Checko, E., Forrester, D. I., Dawud, S. M., Finer, L., Pollastrini, M., Scherer-Lorenzen, M., Valladares, F., Bonal, D., and Gessler, A.: Tree diversity does not always improve resistance of forest ecosystems to drought, Proceedings of the National Academy of Sciences, 111, 14 812–14 815, https://doi.org/10.1073/pnas.1411970111, 2014.

Grossiord, C., Buckley, T. N., Cernusak, L. A., Novick, K. A., Poulter, B., Siegwolf, R. T., Sperry, J. S., and McDowell, N. G.: Plant responses to rising vapor pressure deficit, New Phytologist, 226, 1550–1566, https://doi.org/10.1111/nph.16485, 2020.

Hansen, M. C., Potapov, P. V., Moore, R., Hancher, M., Turubanova, S. A., Tyukavina, A., Thau, D., Stehman, S. V., Goetz, S. J., Loveland, T. R., Kommareddy, A., Egorov, A., Chini, L., Justice, C. O., and Townshend, J. R. G.: High-Resolution Global Maps of 21st-Century Forest Cover Change, Science, 342, 850–853, https://doi.org/10.1126/science.1244693, 2013.

Harpold, A. A., Molotch, N. P., Musselman, K. N., Bales, R. C., Kirchner, P. B., Litvak, M., and Brooks, P. D.: Soil moisture response to snowmelt timing in mixed-conifer subalpine forests, Hydrological Processes, 29, 2782–2798, https://doi.org/10.1002/hyp.10400, 2015.

Hawcroft, M. K., Shaffrey, L. C., Hodges, K. I., and Dacre, H. F.: How much Northern Hemisphere precipitation is associated with extratropical cyclones?, Geophysical Research Letters, 39, 2012GL053 866, https://doi.org/10.1029/2012GL053866, 2012.

Hersbach, H., Bell, B., Berrisford, P., Hirahara, S., Horányi, A., Muñoz-Sabater, J., Nicolas, J., Peubey, C., Radu, R., Schepers, D., Simmons, A., Soci, C., Abdalla, S., Abellan, X., Balsamo, G., Bechtold, P., Biavati, G., Bidlot, J., Bonavita, M., Chiara, G. D., Dahlgren, P., Dee, D., Diamantakis, M., Dragani, R., Flemming, J., Forbes, R., Fuentes, M., Geer, A., Haimberger, L., Healy, S., Hogan, R. J., Hólm, E., Janisková, M., Keeley, S., Laloyaux, P., Lopez, P., Lupu, C., Radnoti, G., de Rosnay, P., Rozum, I., Vamborg, F., Villaume, S., and Thépaut, J. N.: The ERA5 global reanalysis, Quarterly Journal of the Royal Meteorological Society, 146, 1999–2049, https://doi.org/10.1002/qj.3803, 2020.

Hlásny, T., Trombik, J., Bošel'a, M., Merganič, J., Marušák, R., Šebeň, V., Štěpánek, P., Kubišta, J., and Trnka, M.: Climatic drivers of forest productivity in Central Europe, Agricultural and Forest Meteorology, 234-235, 258–273, https://doi.org/10.1016/j.agrformet.2016.12.024, 2017.

IPCC: Climate Change 2021: The Physical Science Basis. Contribution of Working Group I to the Sixth Assessment Report of the Intergovernmental Panel on Climate Change, Cambridge University Press. In Press., 2021.

Jakoby, O., Lischke, H., and Wermelinger, B.: Climate change alters elevational phenology patterns of the European spruce bark beetle (Ips typographus), Global Change Biology, 25, 4048–4063, https://doi.org/10.1111/gcb.14766, 2019.

Kannenberg, S. A., Novick, K. A., Alexander, M. R., Maxwell, J. T., Moore, D. J. P., Phillips, R. P., and Anderegg, W. R. L.: Linking drought legacy effects across scales: From leaves to tree rings to ecosystems, Global Change Biology, 25, 2978–2992, https://doi.org/10.1111/gcb.14710, 2019.

Kennedy, R. E., Yang, Z., and Cohen, W. B.: Detecting trends in forest disturbance and recovery using yearly Landsat time series: 1. LandTrendr — Temporal segmentation algorithms, Remote Sensing of Environment, 114, 2897–2910, https://doi.org/10.1016/j.rse.2010.07.008, 2010.

Kittl, B.: Drought 2018: Beech trees with early discoloured foliage tend to die in subsequent years, https://www.wsl.ch/en/newsseiten/2022/09/drought-2018-beech-trees-with-early-discoloured-foliage-tend-to-die-in-subsequent-years.html, accessed at 25-October-2022, 2022.

McDowell, N. G., Coops, N. C., Beck, P. S., Chambers, J. Q., Gangodagamage, C., Hicke, J. A., ying Huang, C., Kennedy, R., Krofcheck, D. J., Litvak, M., Meddens, A. J., Muss, J., Negrón-Juarez, R., Peng, C., Schwantes, A. M., Swenson, J. J., Vernon, L. J., Williams, A. P., Xu, C., Zhao, M., Running, S. W., and Allen, C. D.: Global satellite monitoring of climate-induced vegetation disturbances, Trends in Plant Science, 20, 114–123, https://doi.org/10.1016/j.tplants.2014.10.008, 2015.

McDowell, N. G., Allen, C. D., Anderson-Teixeira, K., Aukema, B. H., Bond-Lamberty, B., Chini, L., Clark, J. S., Dietze, M., Grossiord, C., Hanbury-Brown, A., Hurtt, G. C., Jackson, R. B., Johnson, D. J., Kueppers, L., Lichstein, J. W., Ogle, K., Poulter, B., Pugh, T. A. M., Seidl, R., Turner, M. G., Uriarte, M., Walker, A. P., and Xu, C.: Pervasive shifts in forest dynamics in a changing world, Science, 368, https://doi.org/10.1126/science.aaz9463, 2020.

Meehl, G. A. and Tebaldi, C.: More intense, more frequent, and longer lasting heat waves in the 21st century, Science, 305, 994–997, https://doi.org/10.1126/science.1098704, 2004.

Messori, G., Wu, M., Vico, G., and Galfi, V. M.: Atmospheric jet stream variability reflects vegetation activity in Europe, Agricultural and Forest Meteorology, 322, 109 008, https://doi.org/10.1016/j.agrformet.2022.109008, 2022.

Mohr, S., Wilhelm, J., Wandel, J., Kunz, M., Portmann, R., Punge, H. J., Schmidberger, M., Quinting, J. F., and Grams, C. M.: The role of large-scale dynamics in an exceptional sequence of severe thunderstorms in Europe May–June 2018, Weather and Climate Dynamics, 1, 325–348, https://doi.org/10.5194/wcd-1-325-2020, 2020.

Nagel, T. A., Mikac, S., Dolinar, M., Klopcic, M., Keren, S., Svoboda, M., Diaci, J., Boncina, A., and Paulic, V.: The natural disturbance regime in forests of the Dinaric Mountains: A synthesis of evidence, Forest Ecology and Management, 388, 29–42, https://doi.org/10.1016/j.foreco.2016.07.047, 2017.

Neumann, M., Mues, V., Moreno, A., Hasenauer, H., and Seidl, R.: Climate variability drives recent tree mortality in Europe, Global Change Biology, 23, 4788–4797, https://doi.org/10.1111/gcb.13724, 2017.

Ogaya, R., Liu, D., Barbeta, A., and Peñuelas, J.: Stem Mortality and Forest Dieback in a 20-Years Experimental Drought in a Mediterranean Holm Oak Forest, Frontiers in Forests and Global Change, 2, https://doi.org/10.3389/ffgc.2019.00089, 2020.

Orth, R., Zscheischler, J., and Seneviratne, S. I.: Record dry summer in 2015 challenges precipitation projections in Central Europe, Scientific Reports, 6, https://doi.org/10.1038/srep28334, 2016.

Pausas, J. G. and Ribeiro, E.: The global fire-productivity relationship, Global Ecology and Biogeography, 22, 728–736, https://doi.org/10.1111/geb.12043, 2013.

Pfahl, S. and Wernli, H.: Quantifying the relevance of atmospheric blocking for co-located temperature extremes in the Northern Hemisphere on (sub-)daily time scales, Geophysical Research Letters, 39, L12 807, https://doi.org/10.1029/2012GL052261, 2012a.

Pfahl, S. and Wernli, H.: Quantifying the Relevance of Cyclones for Precipitation Extremes, Journal of Climate, 25, 6770–6780, https://doi.org/10.1175/JCLI-D-11-00705.1, 2012b.

Rigling, A., Brühlhart, H., Bräker, O. U., Forster, T., and Schweingruber, F. H.: Effects of irrigation on diameter growth and vertical resin duct production in Pinus sylvestris L. on dry sites in the central Alps, Switzerland, Forest Ecology and Management, 175, 285–296, https://doi.org/10.1016/S0378-1127(02)00136-6, 2003.

Rigling, A., Bigler, C., Eilmann, B., Feldmeyer-Christe, E., Gimmi, U., Ginzler, C., Graf, U., Mayer, P., Vacchiano, G., Weber, P., Wohlgemuth, T., Zweifel, R., and Dobbertin, M.: Driving factors of a vegetation shift from Scots pine to pubescent oak in dry Alpine forests, Global Change Biology, 19, 229–240, https://doi.org/10.1111/gcb.12038, 2013.

Rita, A., Camarero, J. J., Nolè, A., Borghetti, M., Brunetti, M., Pergola, N., Serio, C., Vicente-Serrano, S. M., Tramutoli, V., and Ripullone, F.: The impact of drought spells on forests depends on site conditions: The case of 2017 summer heat wave in southern Europe, Global Change Biology, 26, 851–863, https://doi.org/10.1111/gcb.14825, 2020.

Rohner, B., Kumar, S., Liechti, K., Gessler, A., and Ferretti, M.: Tree vitality indicators revealed a rapid response of beech forests to the 2018 drought, Ecological Indicators, 120, 106 903, https://doi.org/10.1016/j.ecolind.2020.106903, 2021.

Rouault, G., Candau, J.-N., Lieutier, F., Nageleisen, L.-M., Martin, J.-C., and Warzée, N.: Effects of drought and heat on forest insect populations in relation to the 2003 drought in Western Europe, Annals of Forest Science, 63, 613–624, https://doi.org/10.1051/forest:2006044, 2006.

Russo, A., Gouveia, C. M., Dutra, E., Soares, P. M. M., and Trigo, R. M.: The synergy between drought and extremely hot summers in the Mediterranean, Environmental Research Letters, 14, 014 011, https://doi.org/10.1088/1748-9326/aaf09e, 2019.

Röthlisberger, M. and Martius, O.: Quantifying the Local Effect of Northern Hemisphere Atmospheric Blocks on the Persistence of Summer Hot and Dry Spells, Geophysical Research Letters, 46, 10 101–10 111, https://doi.org/10.1029/2019GL083745, 2019.

Röthlisberger, M., Pfahl, S., and Martius, O.: Regional-scale jet waviness modulates the occurrence of midlatitude weather extremes, Geophysical Research Letters, 43, 10,989–10,997, https://doi.org/10.1002/2016GL070944, 2016.

Röthlisberger, M., Sprenger, M., Flaounas, E., Beyerle, U., and Wernli, H.: The substructure of extremely hot summers in the Northern Hemisphere, Weather and Climate Dynamics, 1, 45–62, https://doi.org/10.5194/wcd-1-45-2020, 2020.

Rüdisühli, S., Sprenger, M., Leutwyler, D., Schär, C., and Wernli, H.: Attribution of precipitation to cyclones and fronts over Europe in a kilometer-scale regional climate simulation, Weather and Climate Dynamics, 1, 675–699, https://doi.org/10.5194/wcd-1-675-2020, 2020.

Salomón, R. L., Peters, R. L., Zweifel, R., Sass-Klaassen, U. G. W., Stegehuis, A. I., Smiljanic, M., Poyatos, R., Babst, F., Cienciala, E., Fonti, P., Lerink, B. J. W., Lindner, M., Martinez-Vilalta, J., Mencuccini, M., Nabuurs, G.-J., van der Maaten, E., von Arx, G., Bär, A., Akhmetzyanov, L., Balanzategui, D., Bellan, M., Bendix, J., Berveiller, D., Blaženec, M., Čada, V., Carraro, V., Cecchini, S., Chan, T., Conedera, M., Delpierre, N., Delzon, S., L'ubica Ditmarová, Dolezal, J., Dufrêne, E., Edvardsson, J., Ehekircher, S., Forner, A., Frouz, J., Ganthaler, A., Gryc, V., Güney, A., Heinrich, I., Hentschel, R., Janda, P., Ježík, M., Kahle, H.-P., Knüsel, S., Krejza, J., Łukasz Kuberski, Kučera, J., Lebourgeois, F., Mikoláš, M., Matula, R., Mayr, S., Oberhuber, W., Obojes, N., Osborne, B., Paljakka, T., Plichta, R., Rabbel, I., Rathgeber, C. B. K., Salmon, Y., Saunders, M., Scharnweber, T., Sitková, Z., Stangler, D. F., Stereńczak, K., Stojanović, M., Střelcová, K., Světlík, J., Svoboda, M., Tobin, B., Trotsiuk, V., Urban, J., Valladares, F., Vavrčík, H., Vejpustková, M., Walthert, L., Wilmking, M., Zin, E., Zou, J., and Steppe, K.: The 2018 European heatwave led to stem dehydration but not to consistent growth reductions in forests, Nature Communications, 13, 28, https://doi.org/10.1038/s41467-021-27579-9, 2022.

Santos, J. A., Pfahl, S., Pinto, J. G., and Wernli, H.: Mechanisms underlying temperature extremes in Iberia: a Lagrangian perspective, Tellus A: Dynamic Meteorology and Oceanography, 67, 26 032, https://doi.org/10.3402/tellusa.v67.26032, 2015.

Scherrer, D., Bader, M. K.-F., and Körner, C.: Drought-sensitivity ranking of deciduous tree species based on thermal imaging of forest canopies, Agricultural and Forest Meteorology, 151, 1632–1640, https://doi.org/10.1016/j.agrformet.2011.06.019, 2011.

Schubert, S. D., Stewart, R. E., Wang, H., Barlow, M., Berbery, E. H., Cai, W., Hoerling, M. P., Kanikicharla, K. K., Koster, R. D., Lyon, B., Mariotti, A., Mechoso, C. R., Müller, O. V., Rodriguez-Fonseca, B., Seager, R., Seneviratne, S. I., Zhang, L., and Zhou, T.: Global Meteorological Drought: A Synthesis of Current Understanding with a Focus on SST Drivers of Precipitation Deficits, Journal of Climate, 29, 3989–4019, https://doi.org/10.1175/JCLI-D-15-0452.1, 2016.

Schuldt, B., Buras, A., Arend, M., Vitasse, Y., Beierkuhnlein, C., Damm, A., Gharun, M., Grams, T. E., Hauck, M., Hajek, P., Hartmann, H., Hiltbrunner, E., Hoch, G., Holloway-Phillips, M., Körner, C., Larysch, E., Lübbe, T., Nelson, D. B., Rammig, A., Rigling, A., Rose, L., Ruehr, N. K., Schumann, K., Weiser, F., Werner, C., Wohlgemuth, T., Zang, C. S., and Kahmen, A.: A first assessment of the impact of the extreme 2018 summer drought on Central European forests, Basic and Applied Ecology, 45, 86–103, https://doi.org/10.1016/j.baae.2020.04.003, 2020.

Schultz, J.: The Ecozones of the World, Springer Berlin Heidelberg, https://doi.org/10.1007/3-540-28527-X, 2005.

Seftigen, K., Frank, D. C., Björklund, J., Babst, F., and Poulter, B.: The climatic drivers of normalized difference vegetation index and tree-ring-based estimates of forest productivity are spatially coherent but temporally decoupled in Northern Hemispheric forests, Global Ecology and Biogeography, 27, 1352–1365, https://doi.org/10.1111/geb.12802, 2018.

Seidl, R., Schelhaas, M.-J., Rammer, W., and Verkerk, P. J.: Increasing forest disturbances in Europe and their impact on carbon storage, Nature Climate Change, 4, 806–810, https://doi.org/10.1038/nclimate2318, 2014.

Seidl, R., Thom, D., Kautz, M., Martin-Benito, D., Peltoniemi, M., Vacchiano, G., Wild, J., Ascoli, D., Petr, M., Honkaniemi, J., Lexer, M. J., Trotsiuk, V., Mairota, P., Svoboda, M., Fabrika, M., Nagel, T. A., and Reyer, C. P. O.: Forest disturbances under climate change, Nature Climate Change, 7, 395–402, https://doi.org/10.1038/nclimate3303, 2017.

Seidl, R., Honkaniemi, J., Aakala, T., Aleinikov, A., Angelstam, P., Bouchard, M., Boulanger, Y., Burton, P. J., Grandpré, L. D., Gauthier, S., Hansen, W. D., Jepsen, J. U., Jõgiste, K., Kneeshaw, D. D., Kuuluvainen, T., Lisitsyna, O., Makoto, K., Mori, A. S., Pureswaran, D. S., Shorohova, E., Shubnitsina, E., Taylor, A. R., Vladimirova, N., Vodde, F., and Senf, C.: Globally consistent climate sensitivity of natural disturbances across boreal and temperate forest ecosystems, Ecography, 43, 967–978, https://doi.org/10.1111/ecog.04995, 2020.

Seneviratne, S. I., Corti, T., Davin, E. L., Hirschi, M., Jaeger, E. B., Lehner, I., Orlowsky, B., and Teuling, A. J.: Investigating soil moisture–climate interactions in a changing climate: A review, Earth-Science Reviews, 99, 125–161, https://doi.org/10.1016/j.earscirev.2010.02.004, 2010.

Senf, C. and Seidl, R.: Mapping the forest disturbance regimes of Europe, Nature Sustainability, 4, 63–70, https://doi.org/10.1038/s41893-020-00609-y, 2021a.

Senf, C. and Seidl, R.: Persistent impacts of the 2018 drought on forest disturbance regimes in Europe, Biogeosciences, 18, 5223–5230, https://doi.org/10.5194/bg-18-5223-2021, 2021b.

Senf, C. and Seidl, R.: Storm and fire disturbances in Europe: Distribution and trends, Global Change Biology, 27, 3605–3619, https://doi.org/10.1111/gcb.15679, 2021c.

Senf, C., Buras, A., Zang, C. S., Rammig, A., and Seidl, R.: Excess forest mortality is consistently linked to drought across Europe, Nature Communications, 11, 6200, https://doi.org/10.1038/s41467-020-19924-1, 2020.

Sommerfeld, A., Senf, C., Buma, B., D'Amato, A. W., Després, T., Díaz-Hormazábal, I., Fraver, S., Frelich, L. E., Álvaro G. Gutiérrez, Hart, S. J., Harvey, B. J., He, H. S., Hlásny, T., Holz, A., Kitzberger, T., Kulakowski, D., Lindenmayer, D., Mori, A. S., Müller, J., Paritsis, J., Perry, G. L. W., Stephens, S. L., Svoboda, M., Turner, M. G., Veblen, T. T., and Seidl, R.: Patterns and drivers of recent disturbances across the temperate forest biome, Nature Communications, 9, 4355, https://doi.org/10.1038/s41467-018-06788-9, 2018.

Sousa, P. M., Trigo, R. M., Barriopedro, D., Soares, P. M. M., and Santos, J. A.: European temperature responses to blocking and ridge regional patterns, Climate Dynamics, 50, 457–477, https://doi.org/10.1007/s00382-017-3620-2, 2018.

Spensberger, C., Madonna, E., Boettcher, M., Grams, C. M., Papritz, L., Quinting, J. F., Röthlisberger, M., Sprenger, M., and Zschenderlein, P.: Dynamics of concurrent and sequential Central European and Scandinavian heatwaves, Quarterly Journal of the Royal Meteorological Society, 146, 2998–3013, https://doi.org/10.1002/qj.3822, 2020.

Sprenger, M., Fragkoulidis, G., Binder, H., Croci-Maspoli, M., Graf, P., Grams, C. M., Knippertz, P., Madonna, E., Schemm, S., Škerlak, B., and Wernli, H.: Global Climatologies of Eulerian and Lagrangian Flow Features based on ERA-Interim, Bulletin of the American Meteorological Society, 98, 1739–1748, https://doi.org/10.1175/BAMS-D-15-00299.1, 2017.

Stuart-Haëntjens, E., Boeck, H. J. D., Lemoine, N. P., Mänd, P., Kröel-Dulay, G., Schmidt, I. K., Jentsch, A., Stampfli, A., Anderegg, W. R., Bahn, M., Kreyling, J., Wohlgemuth, T., Lloret, F., Classen, A. T., Gough, C. M., and Smith, M. D.: Mean annual precipitation predicts primary production resistance and resilience to extreme drought, Science of The Total Environment, 636, 360–366, https://doi.org/10.1016/j.scitotenv.2018.04.290, 2018.

Tague, C. L., Moritz, M., and Hanan, E.: The changing water cycle: The eco-hydrologic impacts of forest density reduction in Mediterranean (seasonally dry) regions, WIREs Water, 6, https://doi.org/10.1002/wat2.1350, 2019.

Temperli, C., Bugmann, H., and Elkin, C.: Cross-scale interactions among bark beetles, climate change, and wind disturbances: a landscape modeling approach, Ecological Monographs, 83, 383–402, https://doi.org/10.1890/12-1503.1, 2013.

Thom, D., Rammer, W., Garstenauer, R., and Seidl, R.: Legacies of past land use have a stronger effect on forest carbon exchange than future climate change in a temperate forest landscape, Biogeosciences, 15, 5699–5713, https://doi.org/10.5194/bg-15-5699-2018, 2018.

Trenberth, K. E., Dai, A., van der Schrier, G., Jones, P. D., Barichivich, J., Briffa, K. R., and Sheffield, J.: Global warming and changes in drought, Nature Climate Change, 4, 17–22, https://doi.org/10.1038/nclimate2067, 2014.

Trotsiuk, V., Hartig, F., Cailleret, M., Babst, F., Forrester, D. I., Baltensweiler, A., Buchmann, N., Bugmann, H., Gessler, A., Gharun, M., Minunno, F., Rigling, A., Rohner, B., Stillhard, J., Thürig, E., Waldner, P., Ferretti, M., Eugster, W., and Schaub, M.: Assessing the response of forest productivity to climate extremes in Switzerland using model–data fusion, Global Change Biology, 26, 2463–2476, https://doi.org/10.1111/gcb.15011, 2020.

Tucker, C. J.: Red and photographic infrared linear combinations for monitoring vegetation, Remote Sensing of Environment, 8, 127–150, https://doi.org/10.1016/0034-4257(79)90013-0, 1979.

Turco, M., von Hardenberg, J., AghaKouchak, A., Llasat, M. C., Provenzale, A., and Trigo, R. M.: On the key role of droughts in the dynamics of summer fires in Mediterranean Europe, Scientific Reports, 7, 81, https://doi.org/10.1038/s41598-017-00116-9, 2017.

Usbeck, T., Wohlgemuth, T., Dobbertin, M., Pfister, C., Bürgi, A., and Rebetez, M.: Increasing storm damage to forests in Switzerland from 1858 to 2007, Agricultural and Forest Meteorology, 150, 47–55, https://doi.org/10.1016/j.agrformet.2009.08.010, 2010.

Valinger, E. and Fridman, J.: Factors affecting the probability of windthrow at stand level as a result of Gudrun winter storm in southern Sweden, Forest Ecology and Management, 262, 398–403, https://doi.org/10.1016/j.foreco.2011.04.004, 2011.

Vanoni, M., Bugmann, H., Nötzli, M., and Bigler, C.: Quantifying the effects of drought on abrupt growth decreases of major tree species in Switzerland, Ecology and Evolution, 6, 3555–3570, https://doi.org/10.1002/ece3.2146, 2016.

Varol, T. and Ertuğrul, M.: Analysis of the forest fires in the Antalya region of Turkey using the Keetch–Byram drought index, Journal of Forestry Research, 27, 811–819, https://doi.org/10.1007/s11676-016-0235-0, 2016.

Vitasse, Y., Bottero, A., Cailleret, M., Bigler, C., Fonti, P., Gessler, A., Lévesque, M., Rohner, B., Weber, P., Rigling, A., and Wohlgemuth, T.: Contrasting resistance and resilience to extreme drought and late spring frost in five major European tree species, Global Change Biology, 25, 3781–3792, https://doi.org/10.1111/gcb.14803, 2019.

Wernli, H. and Schwierz, C.: Surface Cyclones in the ERA-40 Dataset (1958–2001). Part I: Novel Identification Method and Global Climatology, Journal of the Atmospheric Sciences, 63, 2486–2507, https://doi.org/10.1175/JAS3766.1, 2006.

Westerling, A. L.: Increasing western US forest wildfire activity: sensitivity to changes in the timing of spring, Philosophical Transactions of the Royal Society B: Biological Sciences, 371, 20150 178, https://doi.org/10.1098/rstb.2015.0178, 2016.

Williams, A. P., Allen, C. D., Macalady, A. K., Griffin, D., Woodhouse, C. A., Meko, D. M., Swetnam, T. W., Rauscher, S. A., Seager, R., Grissino-Mayer, H. D., Dean, J. S., Cook, E. R., Gangodagamage, C., Cai, M., and McDowell, N. G.: Temperature as a potent driver of regional forest drought stress and tree mortality, Nature Climate Change, 3, 292–297, https://doi.org/10.1038/nclimate1693, 2013.

Wohlgemuth, T., Kistler, M., Aymon, C., Hagedorn, F., Gessler, A., Gossner, M. M., Queloz, V., Vögtli, I., Wasem, U., Vitasse, Y., and Rigling, A.: Früher Laubfall der Buche während der Sommertrockenheit 2018: Resistenz oder Schwächesymptom?, Schweizerische Zeitschrift fur Forstwesen, 171, 257–269, https://doi.org/10.3188/szf.2020.0257, 2020.

Wolf, G., Brayshaw, D. J., Klingaman, N. P., and Czaja, A.: Quasi-stationary waves and their impact on European weather and extreme events, Quarterly Journal of the Royal Meteorological Society, 144, 2431–2448, https://doi.org/10.1002/qj.3310, 2018.

Wolf, S., Eugster, W., Ammann, C., Häni, M., Zielis, S., Hiller, R., Stieger, J., Imer, D., Merbold, L., and Buchmann, N.: Contrasting response of grassland versus forest carbon and water fluxes to spring drought in Switzerland, Environmental Research Letters, 8, 035 007, https://doi.org/10.1088/1748-9326/8/3/035007, 2013.

Yuan, W., Zheng, Y., Piao, S., Ciais, P., Lombardozzi, D., Wang, Y., Ryu, Y., Chen, G., Dong, W., Hu, Z., Jain, A. K., Jiang, C., Kato, E., Li, S., Lienert, S., Liu, S., Nabel, J. E., Qin, Z., Quine, T., Sitch, S., Smith, W. K., Wang, F., Wu, C., Xiao, Z., and Yang, S.: Increased atmospheric vapor pressure deficit reduces global vegetation growth, Science Advances, 5, https://doi.org/10.1126/sciadv.aax1396, 2019.

Zang, C. S., Buras, A., Esquivel-Muelbert, A., Jump, A. S., Rigling, A., and Rammig, A.: Standardized drought indices in ecological research: Why one size does not fit all, Global Change Biology, 26, 322–324, https://doi.org/10.1111/gcb.14809, 2020.

Zhang, Y., Keenan, T. F., and Zhou, S.: Exacerbated drought impacts on global ecosystems due to structural overshoot, Nature Ecology & Evolution, 5, 1490–1498, https://doi.org/10.1038/s41559-021-01551-8, 2021.

Zscheischler, J. and Seneviratne, S. I.: Dependence of drivers affects risks associated with compound events, Science Advances, 3, 1–11, https://doi.org/10.1126/sciadv.1700263, 2017.

Zschenderlein, P., Fink, A. H., Pfahl, S., and Wernli, H.: Processes determining heat waves across different European climates, Quarterly Journal of the Royal Meteorological Society, 145, 2973–2989, https://doi.org/10.1002/qj.3599, 2019.